Orographic Influences on Rainfall and Track Deflection Associated with the Passage of a Tropical Cyclone

YUH-LANG LIN, DARRELL B. ENSLEY, AND SEN CHIAO

North Carolina State University at Raleigh, Raleigh, North Carolina

CHING-YUANG HUANG

National Central University, Jung-li City, Taoyuan, Taiwan

(Manuscript received 25 October 2001, in final form 1 April 2002)

ABSTRACT

In this study, a nonhydrostatic mesoscale model [Coupled Ocean–Atmosphere Mesoscale Prediction System (COAMPS)] was adopted to simulate Supertyphoon Bilis (2000) and investigate the dynamics of orographic rain and track deflection accompanying the storm as it passes the Central Mountain Range (CMR) of Taiwan. Both the storm track and its associated orographic rainfall distribution are well predicted by the numerical model. The intensity of the storm is underpredicted, resulting in a discontinuous track, due to the lack of specifying a ''bogus'' vortex at the time of model initialization. Cyclonic curvature of the storm track over the island topography track as well as major circulation features are similar to previous studies of landfalling typhoons affecting Taiwan. The model overpredicts the total amount of accumulated rainfall. Generalization of the *flux model* proposed in a 2001 study by Lin and coauthors is used to help predict and understand the observed rainfall distribution by calculating both the orographic and general vertical moisture fluxes from COAMPS model-predicted wind and moisture fields. The vertical moisture flux calculated from the 15-km-resolution simulation compares reasonably well to the actual, storm-observed rainfall distribution. Results of the flux model using 5-km COAMPS model output are not necessarily better than those using the coarser 15-km-resolution results. The overall consistency between the observed rainfall distribution and that predicted by the moisture flux model of Lin and coauthors indicates that the rainfall occurring in the vicinity of the topography was strongly controlled by orographic forcing, rather than being associated with the original rainbands accompanying the typhoon as it moved onshore.

Analysis of simulation control parameters from previous studies of tropical cyclones (TCs) passing over Taiwan's CMR implies that track continuity is strongly linked to V_{max}/Nh and V_{max}/Rf, where V_{max} and R are the maximum tangential wind and radius of the tropical cyclone, N the Brunt–Väisälä frequency, h the maximum mountain height, and f the Coriolis parameter. It appears that track continuity (discontinuity) is associated with higher (lower) values of these two control parameters. Numerical estimates of these two control parameters from observational data and the numerical simulation results for Supertyphoon Bilis produce results consistent with the findings shown here. Physically, V_{max}/Nh represents the vortex-Froude number (linearity) of the outer circulation of the vortex, and V_{max}/Rf represents the intensity (inertial stability) of the vortex. It is hypothesized that when these two control parameters are small, orographic blocking forces a greater percentage of flow around the mountain, instead of allowing the flow to pass over the topography. The vortex becomes unstable, subsequently resulting in a discontinuous surface and near-surface storm track. Analysis of control parameters from previous studies of landfalling typhoons affecting Taiwan also indicates that a westward-moving TC tends to be deflected to the north (south) when V_{max}/Nh is large (small). The dependence of TC track deflection on the basic-flow Froude number (U/Nh) is not revealed by parameter analysis of the previous studies.

1. Introduction

Two major effects of a mesoscale mountain range on the passage of a tropical cyclone (TC) are the generation of heavy orographic rainfall and deflection of the storm track. In this study, we will address these two rather separate issues for typhoons passing over Taiwan's Central Mountain Range (CMR). For the first issue, we will use a mesoscale model to simulate Supertyphoon Bilis (2000) and extend the two-dimensional flux model of orographic rain proposed by Lin et al. (2001) to three dimensions to help improve the realism regarding orographic rainfall prediction. In discussing the second issue, we will estimate flow and orographic parameters from previous studies (e.g., Wang 1980; Chang 1982; Bender et al. 1987; Yeh and Elsberry 1993a,b; Huang

Corresponding author address: Prof. Yuh-Lang Lin, Dept. of Marine, Earth, and Atmospheric Sciences, North Carolina State University at Raleigh, Box 8208, Raleigh, NC 27695-8208.
E-mail: yl_lin@ncsu.edu.

and Lin 1997; Lin et al. 1999; Chiao and Lin 2002, manuscript submitted to *Wea. Forecasting,* hereafter CL02) of the CMR's influence on TC track deflection and propose potential control parameters, which may assess the continuity and deflection of TC tracks. We will then estimate these control parameters from numerical simulations of Supertyphoon Bilis to investigate whether or not they apply to the real case. Similar orographic influences on TC passage have also been observed over the Hispaniola Mountains in the Caribbean Sea, the mountains on Luzon in the Phillippines (Bender et al. 1987), and the Sierra Madre of Mexico (Zehnder and Reeder 1997).

Heavy orographic rainfall may occur much earlier prior to the landfall of a tropical cyclone due to the influence of the mountain range on the conditionally unstable airstream associated with the outer circulation of the cyclone (e.g., Lin et al. 2001; CL02). However, producing an accurate, quantitative precipitation forecast is a particularly difficult challenge. Based on the ingredient argument proposed by Lin et al. (2001), heavy orographic rainfall requires significant contributions from any combination of the following common ingredients: 1) a high precipitation efficiency of the incoming airstream, 2) a low-level jet, 3) a steep mountain, 4) high moisture upstream, 5) favorable mountain geometry (such as a concave geometry) and a confluent flow field, 6) strong synoptically forced upward vertical motion, 7) a large convective system, 8) slow movement of the convective system, and 9) a conditionally or potentially unstable airstream upstream. Based on these common ingredients, we will propose a *flux model of orographic rain* and apply it to the output of real-case simulations of Supertyphoon Bilis (2000) to help improve upon quantitative precipitation prediction and better understand the dynamics of orographically induced precipitation. The finer-resolution data produced by the numerical model will help us better understand the dynamics of orographic rainfall as well as test the proposed model by comparing the model-simulated moisture flux distribution with both observed and model-produced rainfall distributions.

In order to apply the ingredient argument to the prediction of heavy orographic rainfall formation and distribution, the orographically induced moisture flux $(\boldsymbol{V} \cdot \nabla h)q$, where $\boldsymbol{V}$ is the flow impinging on the mountain, h the terrain height, and q the water vapor mixing ratio of the incoming flow, will be used to help predict the orographic rainfall distribution (Lin et al. 2001), which is similar to the methods of Alpert (1986) and Doswell et al. (1996). In this study, this orographic moisture flux, along with a more general vertical moisture flux, wq, will be calculated from the model output and compared with the actual rainfall distributions.

The orographic influence on TC tracks has been studied extensively over Taiwan's CMR due to its almost ideal environment for research: its steepness, its almost north–south (in fact, north-northeast to south-southwest) orientation, and the fact that it is surrounded by oceans and located directly in the path of many typhoons. Wang (1980) showed that the storm center can either cross Taiwan's CMR continuously or discontinuously (also see Chang 1982; Lin et al. 1999; and Wu and Kuo 1999, for recent reviews). For the discontinuous track typhoons, two or more secondary lows tend to form over the lee (west) side of the CMR, one of which eventually develops further and replaces the original low-level low pressure center blocked to the east of the CMR. Hsu and Wang (1960) proposed that a shallow or weak typhoon would dissipate after contact with the Taiwan terrain. For typhoons with maximum sustained winds of about 25–50 m s^{-1}, or if the vertical extent of the circulation is not much more than 6 km, one or more secondary lows may form on the opposite side of the CMR from the landfalling typhoon. Under this situation, the typhoon appears to follow a discontinuous track. For a stronger (maximum sustained wind $>$ 50 m s^{-1}) or deeper (circulation extending to higher than 10.7 km) typhoon, the typhoon center appears to follow a continuous track. Based on numerical sensitivity experiments, Yeh and Elsberry (1993b) found that more intense and rapidly moving vortices are more likely to cross over the mountain and thus maintain a continuous track. Their finding concerning the relationship between vortex intensity and track continuity appears to be consistent with the findings of Hsu and Wang (1960) and Wang (1980). However, the dependence of TC track continuity on the vortex propagation speed was not clearly supported by observations. Thus, it is important to identify the control parameters for track continuity for a TC passing over a mesoscale mountain range. In this study, we will revisit this problem and estimate orographic and flow parameters from previous idealized and real-case simulation studies as well as observational analysis to help identify some control parameters for TC track continuity.

In addition to track continuity, the TC is often deflected when it passes over a mountain range. Although this phenomenon has been studied extensively, diverse results have been found. For example, some studies (e.g., Chang 1982; Bender et al. 1987) indicate that a westward-moving typhoon tends to be deflected northward upstream of Taiwan, subsequently moving cyclonically over the CMR, while others (e.g., Yeh and Elsberry 1993a; Huang and Lin 1997; Lin et al. 1999) found a southward deflection upstream of Taiwan's CMR. If one inspects the extensive observational analysis of typhoon tracks made by Wang (1980), the majority of typhoons with continuous tracks do deflect southward upstream of Taiwan, subsequently passing over the CMR in a cyclonic fashion. Similar southerly deflections of storm tracks have also been found for hurricanes passing over a larger-scale mountain, such as the Sierra Madre of Mexico, from numerical experiments using a shallow-water model (Zehnder 1993; Zehnder and Reeder 1997). Physical factors influencing the northward or southward deflection include blocking and modification of the basic (steering) flow, interaction of the TC's circulation with orography, TC intensity, translation speed of the TC, the ''ventilation mechanism'' (Yeh and Elsberry 1993a), and cumulus heating (Chang 1982). Therefore, this topic deserves further study. In this paper, we plan to identify control parameters for determining the storm track deflection by analyzing the flow and orographic parameters used in previous studies.

This paper is organized as follows. Section 2 will discuss the synoptic environments, the Coupled Ocean–Atmosphere Mesoscale Prediction System (COAMPS) model configuration and description of the numerical experiments, in addition to the control case Supertyphoon Bilis simulation. In section 3, we will investigate the orographic influence on simulated rainfall and compare the simulation results with those from a flux model. In section 4, we will identify the control parameters for track continuity and deflection for TCs passing over Taiwan from previous studies and apply the parameters to Supertyphoon Bilis and our numerically simulated storm. Concluding remarks are made in section 5.

2. Numerical simulations of Supertyphoon Bilis

a. Synoptic environment

Supertyphoon Bilis (2000) is almost ideal for case study, as it followed a very straight track as it approached Taiwan. This storm was a very intense, category-5 typhoon with a minimum central pressure of 915 hPa as it made landfall along the southeast coast of Taiwan near Tai-Tung [(23.1°N, 121.4°E); see Figs. 1 and 3)] around 1400 UTC 22 August 2000 (hereafter denoted as 8/22/14UTC). It produced maximum winds of 75 m s^{-1} and heavy rainfall (949 mm in 20 h measured at Yu-Li, Hua-Lian County (in northeast Taiwan). Supertyphoon Bilis also caused at least 11 deaths in Taiwan. Just before landfall, Bilis turned north and followed a cyclonic track across the island (Fig. 4), which is similar to that found in many previous observational and idealized studies of tropical cyclones passing over Taiwan (e.g., Wang 1980; Chang 1982; Bender et al. 1987). Satellite imageries (not shown) indicated a well-defined eye as Bilis approached Taiwan, which was not detectable after making landfall due to the asymmetric circulation induced by the island's orography. Bilis further weakened significantly after passing over Taiwan's CMR.

Figure 1a shows the NOGAPS-analyzed surface chart at 8/22/00UTC 2000, which depicts the synoptic environments across eastern Asia and the northwestern Pacific Ocean. The synoptic environment consisted of Tropical Storm Kaemi moving along the central coast of Vietnam before making landfall and dissipating inland of the Indo-China peninsula, and persistent, but spatially small, areas of high pressure north and northeast of Supertyphoon Bilis that moved generally westward. These high pressure systems, along with Tropical Storm Kaemi and the North Pacific high, tended to help advect or steer Bilis northwestward toward Taiwan. Several high and low pressure areas were also shown to the north of 40°N, which apparently did not seem to play much of a role in influencing the storm track of Supertyphoon Bilis. In addition to the major synoptic features shown at the surface, a low-level jet (LLJ) can clearly be seen on the 700-hPa chart (Fig. 1b), which was associated with the outer circulation of Supertyphoon Bilis. Similar to many previous heavy orographic rainfall events in the subtropics and midlatitudes, this LLJ has a significant impact on the formation of heavy orographic rainfall over the eastern slopes of the CMR since it tends to induce strong upward vertical motion over the windward slopes in a conditionally unstable flow (Lin et al. 2001). Associated with this LLJ, a moist tongue of air extended from the Bilis's low pressure center into southeastern Taiwan. The synoptic systems at 700 hPa were similar to those at the surface. The 700-, 500-, and 300-hPa charts (Figs. 1b–d) show a high pressure system located to the east of China and north of Taiwan at 8/22/00UTC that subsequently moved southeastward to the east of Taiwan by the time Bilis made landfall in China. The easterly or southeasterly flow to the east of Taiwan helped to steer Bilis northwestward toward Taiwan. There appears to be generally easterly-southeasterly flow east of Taiwan throughout the entire troposphere during this time period.

b. Model configuration and description of experiments

The NOGAPS reanalyzed dataset is employed to initialize the numerical simulations. The model used in this study is the Naval Research Laboratory's COAMPS. A detailed description of the model can be found in Hodur (1997). COAMPS is a nonhydrostatic, fully compressible, three-dimensional model with a detailed data assimilation scheme. Subgrid-scale moist convective processes are parameterized by the Kain and Fritsch (1993) cumulus parameterization scheme, while the grid-scale evolution of the moist processes are explicitly predicted from microphysical budget equations following Rutledge and Hobbs (1983), which is related to the Lin–Farley–Orville scheme (Lin et al. 1983). Planetary boundary layer processes are parameterized by the level-2.5 formulations of Therry and LaCarrere (1983), and longwave and shortwave radiation processes are parameterized following Harshvardhan et al. (1987).

The domain configuration is shown in Fig. 2a. Three nested domains of 45-km (91 $\times$ 101), 15-km (151 $\times$ 151), and 5-km (133 $\times$ 133) horizontal resolution were used, along with 30 layers in the vertical, 11 of which are below 2 km for higher vertical resolution near the surface. Figure 2b shows the model's 5-km resolution of the 1-km terrain used in this study, which provides

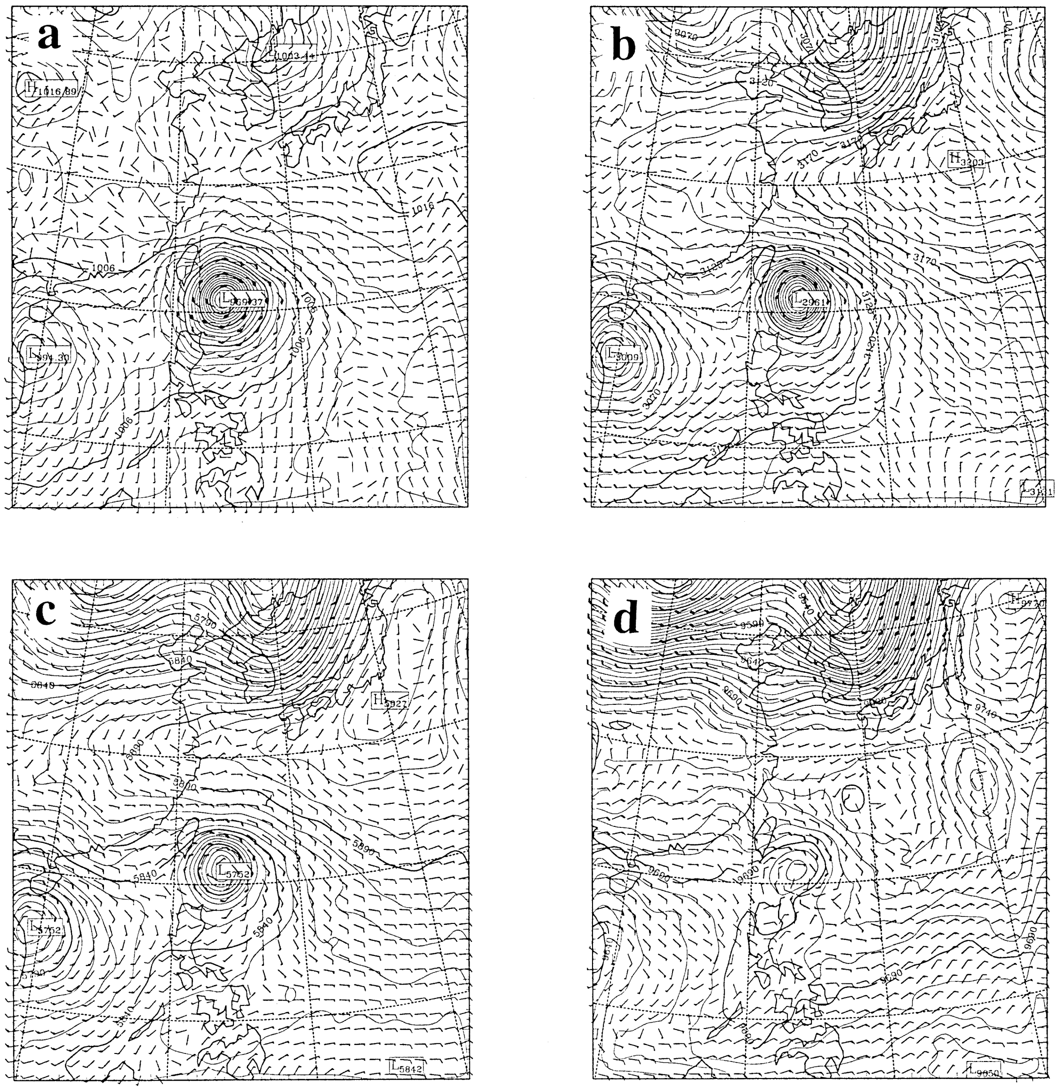

FIG. 1. Wind vectors and pressure or height fields from the NOGAPS reanalysis data at 0000 UTC 22 Aug (8/22/00UTC) 2000 for (a) surface, (b) 700, (c) 500, and (d) 300 hPa.

a much higher terrain resolution than that used in most previous studies. A 1-km resolution land-use dataset (not shown) has also been used in this study. The initialization procedure and data assimilation cycling routine used by COAMPS are summarized in Table 1. In the table, *cold start* (CS) refers to a COAMPS simulation that is initialized from the $1.0° \times 1.0°$ NOGAPS global model dataset, while *warm start* (WS) refers to a COAMPS simulation that is restarted from a previous COAMPS simulation using NOGAPS boundary conditions. In one simulation, there may be multiple warm starts, limited only by the frequency of observed data for the data assimilation cycle, which is every 12 h for our numerical simulations.

Two sets of experiments, namely, control experiments (CON) and no-terrain experiments (NT), were performed. Both CON and NT experiments were initialized with a cold start at 8/21/12UTC and integrated in time for 60 h. Each experiment consisted of several restarted simulations (i.e., WSs). In these experiments, the simulated storm Bilis made landfall approximately 26 h after the initialization time. Both sets of experiments have three horizontal grid meshes of 45 km (coarse), 15 km (middle), and 5 km (inner), which were required to be initialized and integrated at the same time. Thus, there are a total of six numerical simulations, namely, CON-45, CON-15, CON-5, NT-45, NT-15, and NT-5. Most of the analyses performed are based on the 15-km simulations from each set of experiments, that is, CON-15 and NT-15. Each individual simulation will be denoted likewise hereafter. Some of the 5-km simulation results have also been analyzed, providing better and finer details around the time of simulated landfall in Taiwan.

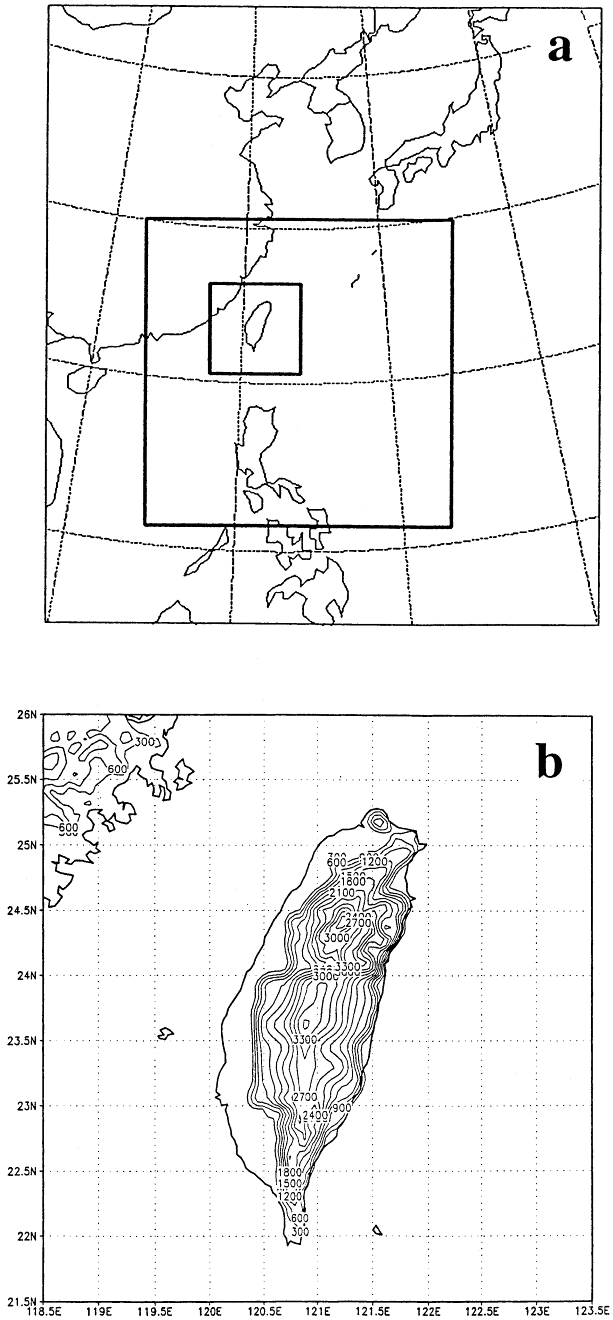

FIG. 2. (a) Domain configuration for COAMPS model simulations used in this study. Three domains (outer, middle, and inner) were adopted; (b) the model's 5-km resolution of the 1-km terrain databases used in this study.

c. The control experiment (CON)

The control numerical simulations failed to capture the observed intensity of Supertyphoon Bilis (2000), which was due to the fact that the simulations initialized with the NOGAPS reanalysis data started without implementing a bogus vortex. As shown in Fig. 1a, the NOGAPS analyzed minimum central pressure for the storm at 8/22/00UTC was 969.37 hPa, which had subsequently deepened from 984.52 hPa at 8/21/21UTC (not shown). These central pressures represent category-1 and -2 tropical cyclones, respectively, although the NOGAPS analyzed wind fields never quite captured the actual, observed strength of the typhoon. At both of these times, Supertyphoon Bilis was a very intense category-5 storm with an observed minimum central pressure of 920 hPa (Fig. 3a). In our numerical simulations, we did not apply any "bogusing schemes" to the initial vortex. Thus, the central pressure of these simulations at 8/22/03UTC was about 60–65 hPa too high to begin with (Fig. 3a) and the maximum surface wind speed was about 28 m s^{-1}, which is about 44 m s^{-1} weaker than the actual observed surface wind (Fig. 3b). Note that the intense vortex (920 hPa) was not well represented by the 1° NOGAPS dataset used for model initialization. The lowest numerically simulated central pressure for CON-15 was slightly higher than 977 hPa, with a landfall intensity of between 980 and 985 hPa (vs the 915-hPa observed central pressure at landfall) at 8/22/15UTC (Fig. 3a). At landfall (8/22/15UTC), the CON-15 simulated maximum surface wind speed is about 35 m s^{-1}, compared with the actual surface observed maximum wind speed of about 68 m s^{-1} (Fig. 3b). Although the intensity of the simulated typhoon is too weak compared with the observed storm, it may serve as a basis for sensitivity tests for examining the orographically induced track continuity and deflection, as well as observed rainfall rates for weak to moderate typhoons.

The typhoon tracks from the control experiment (CON-15) and that observed for Supertyphoon Bilis are superimposed in Fig. 4. Although the track of the parent storm associated with the cold start simulation (not shown) exhibited some wobbling for the first 9–12 h due to the model spinup process, it eventually settled on a consistently northwestward track, while the CON-15 storm quickly settled back to a very similar track as

TABLE 1. Initialization and data assimilation cycling of COAMPS.

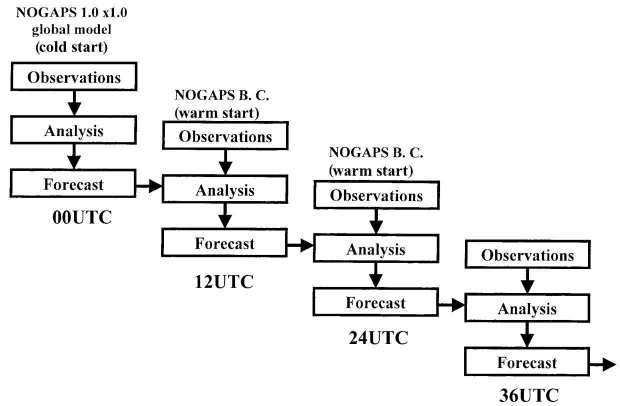

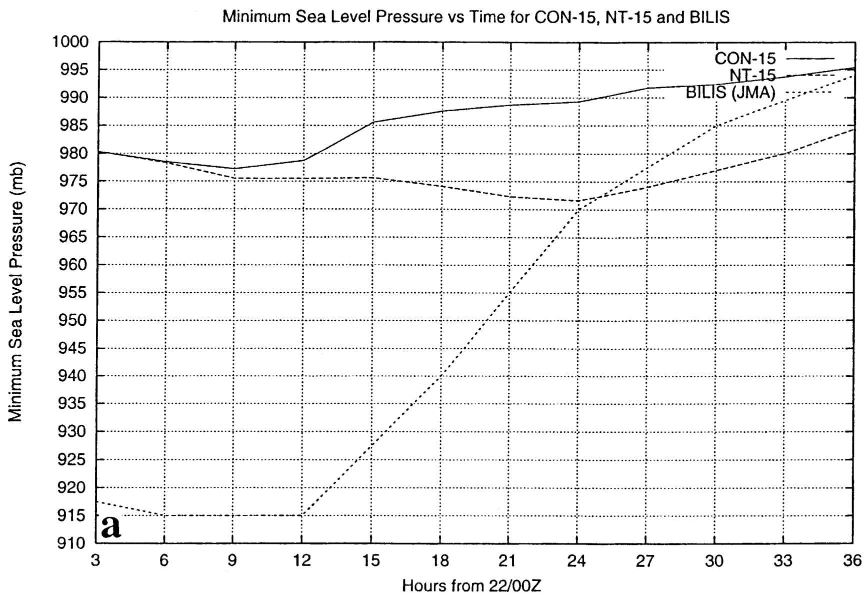

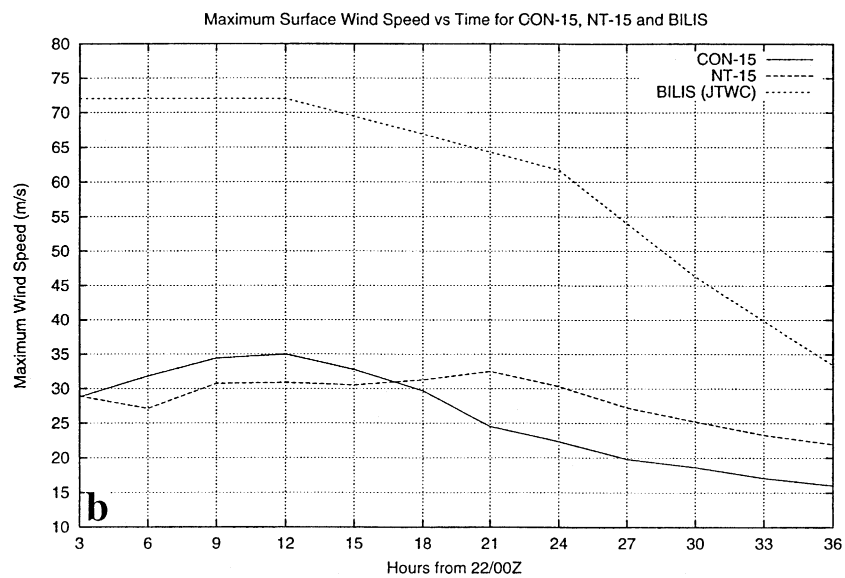

FIG. 3. Time evolutions of (a) min pressures and (b) max wind speeds for cases CON-15 (solid line) and NT-15 (dashed line). The JTWC used 1-min average values for sustained winds and also listed the pressure data from JMA. Landfall of Bilis occurred at about 8/22/15UTC.

that observed throughout the rest of the life of the actual storm. Both storms (Bilis and CON-15) exhibited the characteristic northward deflection when they approached Taiwan, with a turn to the southwest after passing over the CMR before resuming a northwestward track toward China. In other words, *the CON-15 storm turned cyclonically when it passed over the CMR, similar to results found in some previous studies* (e.g. Wang 1980; Chang 1982; Bender et al. 1987, Wu 2001).

While the actual Supertyphoon Bilis maintained a continuous track crossing the CMR, the numerically simulated CON-15 storm track was discontinuous (Fig. 4), with a secondary low pressure center forming over the northwestern part of the island at 8/22/15UTC, subsequently strengthening and becoming the primary low pressure center after 8/22/18UTC as it left Taiwan. Overall, the CON-15 simulated track agrees quite well with the observed track (Fig. 4). As found in previous studies, the surface low to the northwest of Taiwan was formed by adiabatic warming and vorticity stretching associated with the downslope winds. Above the surface, the low pressure center followed a more continuous track, with much less pronounced northward deflection across the island (Fig. 5a). At the surface and

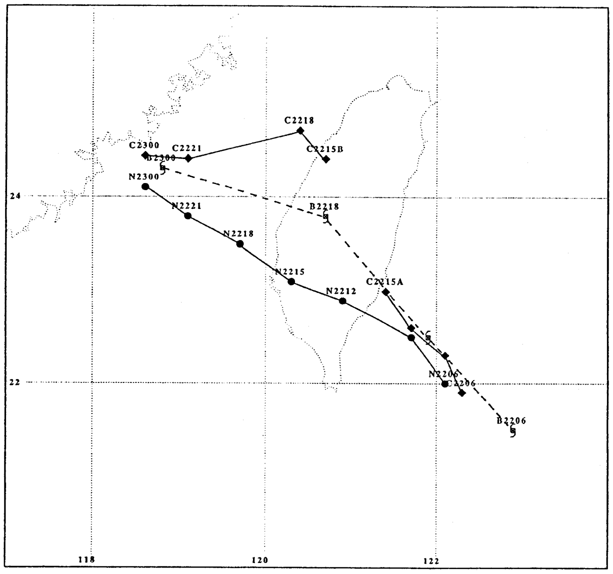

FIG. 4. Supertyphoon Bilis tracks from (a) observation (TC symbols, every 6 h), (b) CON-15 (diamonds, every 3 h), and (c) NT-15 (circle, every 3 h).

500 hPa at 8/22/15UTC, two low pressure centers coexisted on both the upstream and downstream sides of the mountain range, while the simulated CON-15 storm was crossing over the CMR. In addition, there was a noticeable lack of vertical phase coherence of these low pressure centers throughout the simulation (Fig. 5a). The same was generally true of the circulation centers (Fig. 5b) at the major isobaric levels (700, 500, and 300 hPa) and between the low pressure and circulation centers at each level (cf. Figs. 5a,b). The tracks of the circulation centers were continuous when the simulated CON-15 storm was crossing over the CMR except on the surface at 8/22/15UTC, which was due to the formation of a secondary vortex while the parent storm was blocked upstream of the mountain. The blocked flow upstream then circulated around the northern part of the CMR, helping to form the secondary vortex to the southwest. As noted in Lin et al. (1999), the low pressure and circulation centers tend to split when a tropical cyclone passes over the CMR, which makes it difficult to trace the path of the storm center. The current numerical simulations also show this behavior. For example, the surface secondary low is located to the northwest of the CMR, while the surface circulation center is located to the southwest.

Figure 6 shows the pressure and vector wind fields when the simulated CON-15 storm was passing over the CMR. At 8/22/12UTC, the simulated storm approached the southeast coast of Taiwan with coherent low pressure centers aligned in the vertical (left panels of Fig. 6). At the surface, there was an inverted pressure ridge located over the northeastern slope of the CMR due to an upstream high pressure perturbation generated by the mountain located in part of the storm's outer

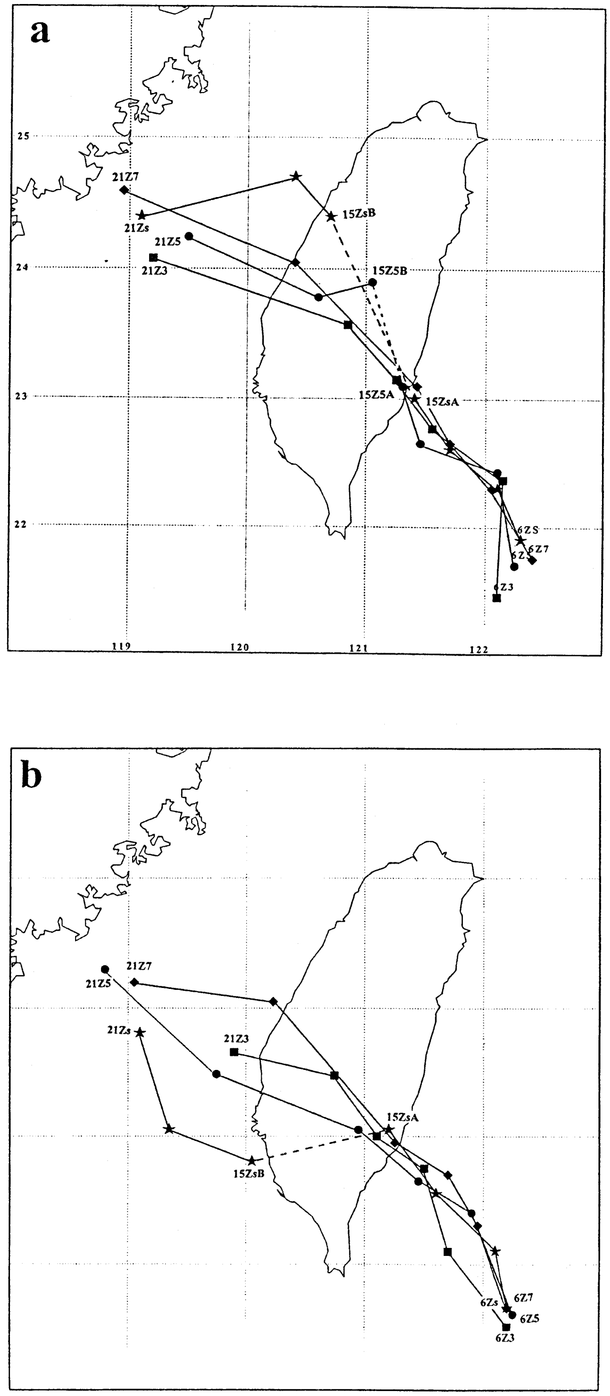

FIG. 5. Simulated (a) low centers and (b) circulation centers for Supertyphoon Bilis in CON-15. Centers at surface (stars), 700 (diamonds), 500 (circles), and 300 hPa (squares) are shown in both panels. The letter Z denotes UTC and the number before it denotes the hour in UTC on 22 Aug. The symbols s, 7, 5, and 3 after "Z" denote surface, 700, 500, and 300 hPa, which are followed by A or B if the center coexists on both upstream and downstream of the CMR. The time interval for the low centers plotted is 3 h.

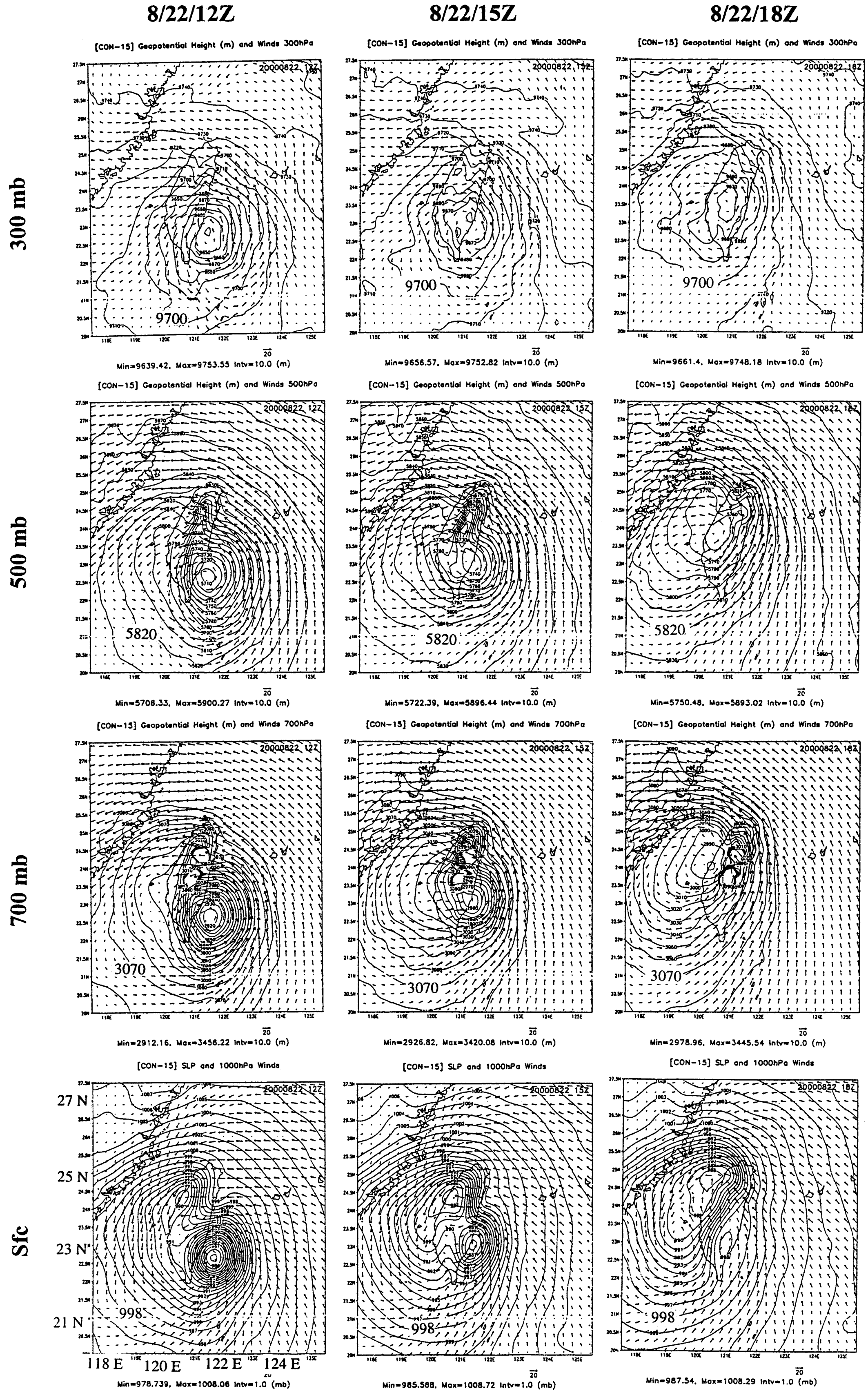
8/22/12Z
8/22/15Z
8/22/18Z
300 mb
500 mb
700 mb
Sfc
[CON-15] Geopotential Height (m) and Winds 300hPa
Min=9639.42, Max=9753.55 Intv=10.0 (m)
Min=9656.57, Max=9752.82 Intv=10.0 (m)
Min=9661.4, Max=9748.18 Intv=10.0 (m)
[CON-15] Geopotential Height (m) and Winds 500hPa
Min=5708.33, Max=5900.27 Intv=10.0 (m)
Min=5722.39, Max=5896.44 Intv=10.0 (m)
Min=5750.48, Max=5893.02 Intv=10.0 (m)
[CON-15] Geopotential Height (m) and Winds 700hPa
Min=2912.16, Max=3456.22 Intv=10.0 (m)
Min=2926.82, Max=3420.08 Intv=10.0 (m)
Min=2978.96, Max=3445.54 Intv=10.0 (m)
[CON-15] SLP and 1000hPa Winds
Min=978.739, Max=1008.06 Intv=1.0 (mb)
Min=985.588, Max=1008.72 Intv=1.0 (mb)
Min=987.54, Max=1008.29 Intv=1.0 (mb)
9700
5820
3070
998
27 N
25 N
23 N
21 N
118 E
120 E
122 E
124 E

circulation, which has a strong component perpendicular to the CMR. Concurrently, there was a strong, *secondary low* produced over the northwestern coast of Taiwan, which was generated by vorticity stretching and the adiabatic warming associated with the strong downslope wind as part of the storm circulation over the northern portion of the CMR, similar to that found in idealized simulations (Chang 1982; Lin et al. 1999). This secondary low covers a large area of the lee (western) slope, has several embedded lows in the 5-km simulations (not shown), and is consistent with observations of other typhoons (e.g., Wang 1980). At 700 hPa (Fig. 6), the parent low was almost collocated with the surface low. However, there was no strong secondary low produced on the lee (western) side of the mountain due to the fact that most of the incoming flow was able to pass over the mountain at this level since the secondary low was shallow (generally <3 km). At both 500 and 300 hPa (Fig. 6), the northern portion of the CMR was under the influence of an inverted trough and ridge, respectively. This inverted low and high pressure perturbation was indicative of a hydrostatic wave response to orographic forcing occurring along Bilis's outer circulation (e.g., see Smith 1979; Lin 1993). A similar vertical flow response has also been shown in the numerical simulations of Typhoon Herb (1996) (Kuo and Wang 1997).

In between the northwestern mountains of Taiwan and southeastern mountains of China, the outer circulation of Supertyphoon Bilis was channeled through the coastal mountains on both sides of the Taiwan Strait and formed a *northeasterly gap flow* or *barrier jet* (first row of Fig. 7). This type of gap flow or barrier jet has also been observed over other mountain ranges, such as Gibraltar (Scorer 1952), the Strait of Juan de Fuca (Overland and Walter 1981), and northwestern Taiwan under southwesterly monsoonal flow during the Mei-Yu season (e.g., Chen and Li 1995). One significant effect of this gap flow between the Taiwanese and Chinese coastal mountain ranges is to strengthen the formation of the secondary vortex along the southwestern lee side of the CMR. This is clearly shown in the surface relative vorticity fields (Fig. 7). Another interesting phenomenon is the *easterly gap flow* passing through the two highest peaks of the CMR, as shown in the 700-hPa plots at 8/22/12UTC and 15UTC (third row of Fig. 6). This easterly gap flow also strengthened the secondary lee vortex immediately to the south (third row of Fig. 7). At 300 hPa in addition to the hydrostatic mountain waves, the overall ambient flow is less disturbed by the orography (Figs. 6, 7) and passes over the topography in a much straighter path (Fig. 5).

At 8/22/15UTC, Bilis has made landfall along the southeastern coast of Taiwan, which is clearly depicted in the 300-hPa plots (first rows of Figs. 6, 7). The 500- and 700-hPa low pressure centers were blocked by the mountains and remained over the east coast of Taiwan, while a secondary surface low developed in northwestern Taiwan to be as strong as the parent low located in southeastern Taiwan (fourth row of Fig. 6). Banners of positive and negative relative vorticities, which were produced by the mountain gaps and peaks, are present at 700 hPa at this time (Fig. 7). Similar features, which are often presented as potential vorticity (PV) banners, have been simulated and observed over the European Alps. A secondary vortex formed along the southwestern coast of Taiwan at this time (second column of Fig. 7), when the tracks of both the low pressure and vorticity centers of the CON-15 storm were discontinuous, as depicted by the coexistence of the parent and secondary (leeside) storm centers. Note that the observed tracks of Bilis's low pressure and circulation centers were continuous since the intensity of the actual storm is much stronger than the simulated control case storm (CON-15).

Due to the lack of vertical coherence between the secondary low and vortex centers at different levels during Bilis's passage over Taiwan, the secondary low and secondary vortex appear as an elongated cyclone on the lee side of the CMR at 500 and 700 hPa, and the surface at 8/22/18UTC (third column of Figs. 6, 7), while the pressure and vorticity patterns retain their integrity at 300 hPa. At this time, the circulation symmetry of the typhoon was destroyed by the mountain range and the eye was no longer identifiable in the satellite imagery (not shown). At later times, the upper-level parent cyclone was able to help the elongated surface–500-hPa cyclone spin up and get organized into a coherent circulation as it was heading toward China.

Storm CON-15 deepened to 977 hPa but never reached Bilis's observed 915 hPa at the time of landfall in Taiwan. The simulated storm accelerates over the island, but only very close to landfall ($\sim$1–3 h before). This is similar to previous studies, although some show acceleration up to 12 h prior to landfall (e.g., Bender et al. 1987). Another difference from previous studies is the changes in storm intensity before, during, and after landfall. Orographic effects on simulated rainfall will be discussed in section 3.

d. No-terrain experiment (NT)

The no-terrain experiment with 15-km resolution (NT-15) was initialized at the same time as CON-15, that is, 8/21/12UTC, when the observed storm was only

←

FIG. 6. Horizontal vector wind fields and pressure (height for higher levels) fields at 8/22/12UTC, 15UTC, 18UTC, and 21UTC 2000 for (a) surface, (b) 700, (c) 500, and (d) 300 hPa. The contours of 998 hPa, 3070 m, 5820 m, and 9700 m are denoted on surface, 700-, 500-, and 300-hPa fields, respectively. The contour values are 1 hPa on the surface fields and 10 m on the upper-air fields.

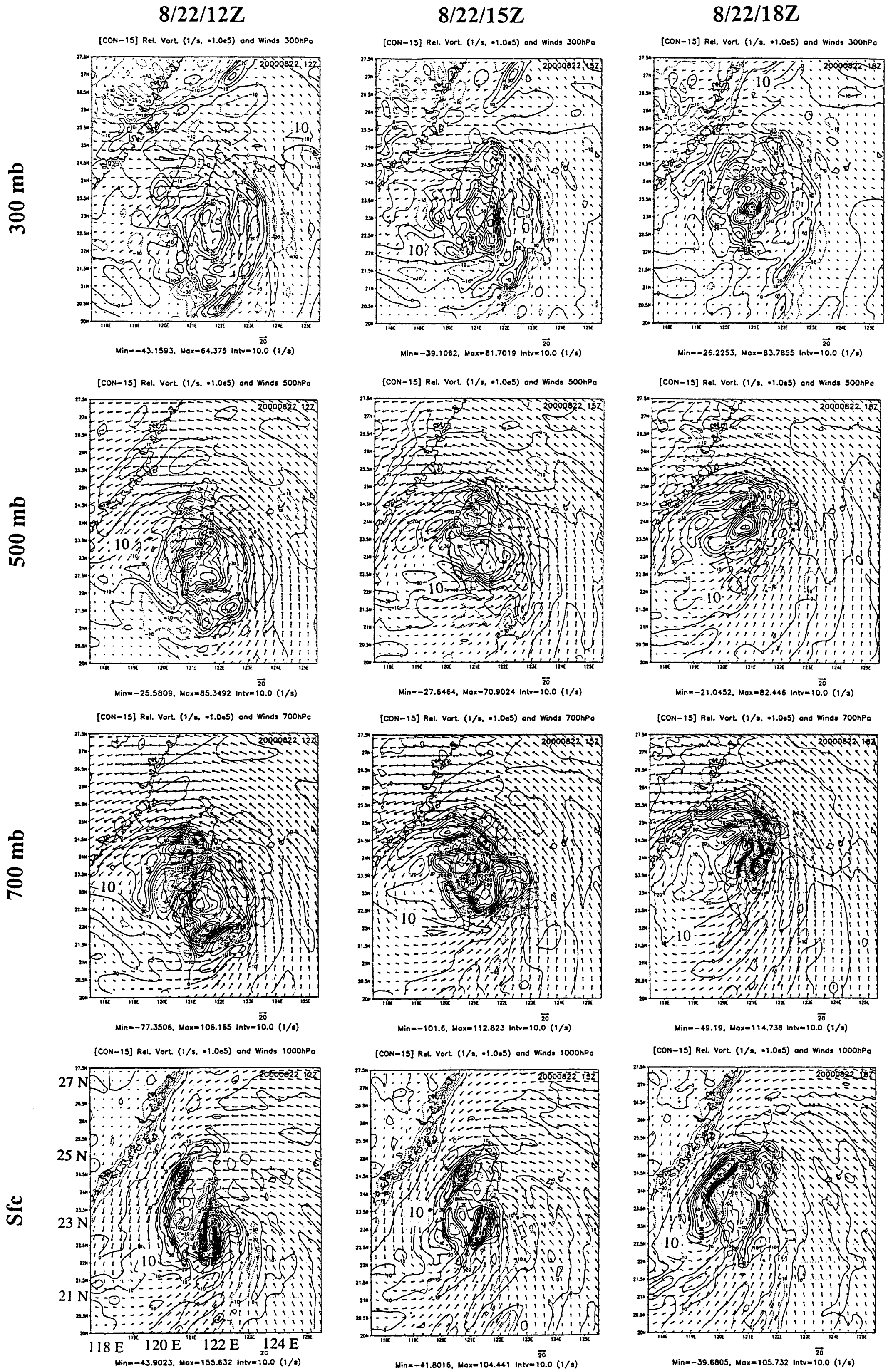

FIG. 7. Same as Fig. 6 except for horizontal vector wind fields and relative vorticity fields. The contours of 10 m s^{-1} wind speed are denoted in each panel. The contour interval of wind speed is 10 m s^{-1} in all panels.

920 hPa, so the starting point for both experiments is the same. Unlike storm CON-15, which deepened to only 977 hPa prior to landfall, storm NT-15 continued to slowly deepen even as it crossed over the flat island, reaching a minimum central pressure of 972 hPa by 8/23/00UTC, about 3 h before making landfall in China (Fig. 3a). The main reason that storm NT-15 continues to deepen (compared to the CON-15 storm) was due to *the lack of asymmetric flow induced by the orography*. The maximum surface wind speed of storm NT-15 was also stronger than storm CON-15 (Fig. 3b). In addition to being slightly stronger than storm CON-15, storm NT-15 also exhibited a much greater vertical coherence between the low pressure and circulation centers (not shown).

The track of NT-15's low pressure centers is shown in Fig. 4, along with those of CON-15 and of the observed typhoon. The simulated storm NT-15 exhibited an almost straight continuous track across the southern end of the island (as there was obviously no orography to affect the storm), thus no blocking of the steering flow or the storm circulation. The track of storm NT-15 did show a slight northward deflection by 8/22/09UTC just prior to landfall, and the storm track curved slightly southward as it passed over the island and out over the Taiwan Strait. This slight deflection was most likely due to the influence of the planetary boundary layer friction when the storm passed over the flat land surface. Even though storm NT-15 was moving faster than storm CON-15 when it approached Taiwan (it also made landfall about 4 h earlier), storm CON-15 seemed to ''catch up'' with storm NT-15 as the secondary surface low formed to the northwest and became the new primary low pressure center.

3. Orographic influence on rainfall and a flux model of orographic rain

Figure 8a shows the observed 24-h precipitation for 22 August 2000. The major rainfall region occupied almost the entire east coast of Taiwan, with two major maximum rainfall areas located at both the northern and southern ends. The maximum 24-h accumulated rainfall reached totals of about 600 mm (480 mm) in the northern (southern) region. In addition to these two major rainfall maxima, three additional local rainfall maxima (with smaller total rainfall amounts) also existed southwest of the southern region of major maximum rainfall. The numerically simulated precipitation for the same 24-h period is shown in Fig. 8b. Although the simulated rainfall intensity (with a maximum value of 620 mm) was only slightly greater than the observed rainfall intensity (with a maximum value of 600 mm), the quantitative precipitation was considerably overpredicted because the simulated storm (CON-15) is much weaker than the actual storm. However, the overall rainfall distribution compared well with the observed distribution except for the simulated rainfall in southern Taiwan, which was not shown in the observations. Although the rainfall area over the east coast of Taiwan was reasonably well predicted by the CON-15 simulation, the detailed maximum rainfall regions along the east coast of Taiwan were not well predicted. The CON-15 simulated rainfall maxima extended over the ocean, which roughly reflected the northern and southern flanks of the rainbands associated with Supertyphoon Bilis.

Figure 8c shows the simulated 24-h accumulated precipitation from the 5-km-resolution control run (CON-5). Unlike the coarser CON-15 simulation, the precipitation distribution from this simulation did exhibit three distinct rainfall maxima over the east coast of Taiwan. The northern and southern rainfall maxima agreed reasonably well with the observed rainfall maxima (Fig. 8a). Similar to the CON-15 simulation, the observed maximum rainfall area over the southern peninsula of Taiwan was not predicted. Over the southwestern coast, an area of maximum rainfall, which extended farther into the Taiwan Strait, was also simulated. This rainfall area corresponded to the area of maximum rainfall located near the southwestern concave region of the CMR, although the total observed rainfall in this area was less than that predicted. The numerically simulated rainband over the southwestern coast of Taiwan and the adjacent ocean areas was caused by the southwesterly flow associated with the outer circulation of Bilis. Although the CON-5 simulation did a better job in predicting the rainfall distribution than that of the CON-15 simulation, the maximum predicted rainfall amount is extremely high ($\sim$1212 mm). This problem in overpredicting the total simulated rainfall might be propagated from the coarser-resolution CON-15 (15 km) simulation to the finer-resolution CON-5 (5-km) simulation, which might result from parameterization misrepresentation of actual cumulus convection and microphysical processes occurring in the vicinity of mesoscale mountains.

Figures 9a,b show the observed 3-h accumulated precipitation (in millimeters) valid for the periods of 8/22/12–15UTC and 15–18UTC, respectively. The corresponding simulated (CON-15) precipitation distributions are also displayed in Figs. 9c,d. During these two time periods, the precipitation distributions indicate a dipole pattern over the east coast of Taiwan. During 12–15UTC, the CON-15 predicted rainfall (Fig. 9c) has two maxima, one located over the central east coast and the other located over the southern peninsula of Taiwan. The simulated rainfall distribution over the east coast roughly agrees with the overall observed pattern (Fig. 9a), but not in the detailed distribution of rainfall. The rainfall over the southern peninsula was not shown in the observations (Fig. 9a) and is overpredicted by CON-15.

During 15–18UTC, the CON-15 predicted rainfall distribution (Fig. 9d) also roughly agrees with the overall observed pattern (Fig. 9b), especially with the northward propagation of the maximum rainfall over the east coast of Taiwan. This northward propagation of both

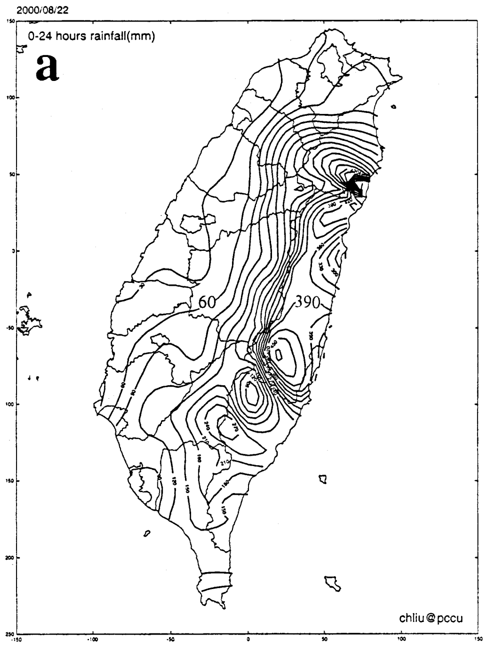

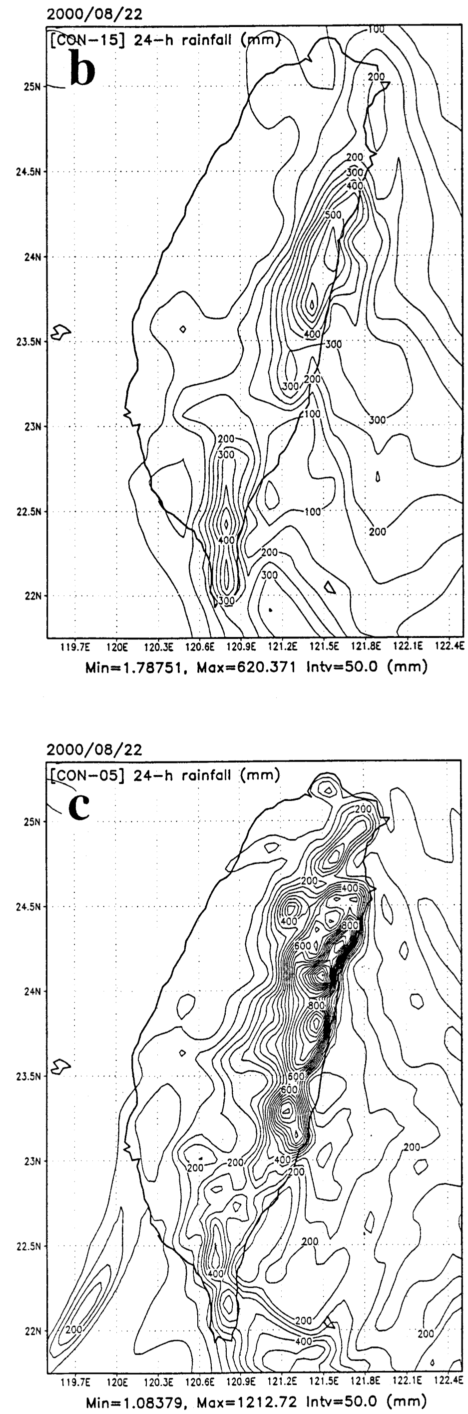

FIG. 8. (a) Observed, (b) 15-km simulated (CON-15), and (c) 5-km simulated (CON-5) 24-h accumulated precipitation (in mm) for 22 Aug 2000: (a) the contour interval is 30 mm, and the max 24-h accumulated rainfall reached an amount of about 600 mm (480 mm) at the northern (southern) end of this maximum rainfall region.

the observed and predicted maximum rainfall was apparently associated with the northwestward movement of Bilis when it passed over the island during this time period (Fig. 6).

As mentioned in the introduction, Lin et al. (2001) recently proposed that heavy orographic rainfall requires significant contributions from any combination of the following common ingredients: 1) high precipitation efficiency of the incoming airstream, 2) a low-level jet, 3) a steep mountain, 4) high moisture upstream, 5) favorable mountain geometry (such as a concave geometry) and a confluent flow field, 6) strong synoptically forced upward vertical motion, 7) a large convective system, 8) slow movement of the convective system, and 9) a conditionally or potentially unstable upstream airstream. The synoptic and mesoscale

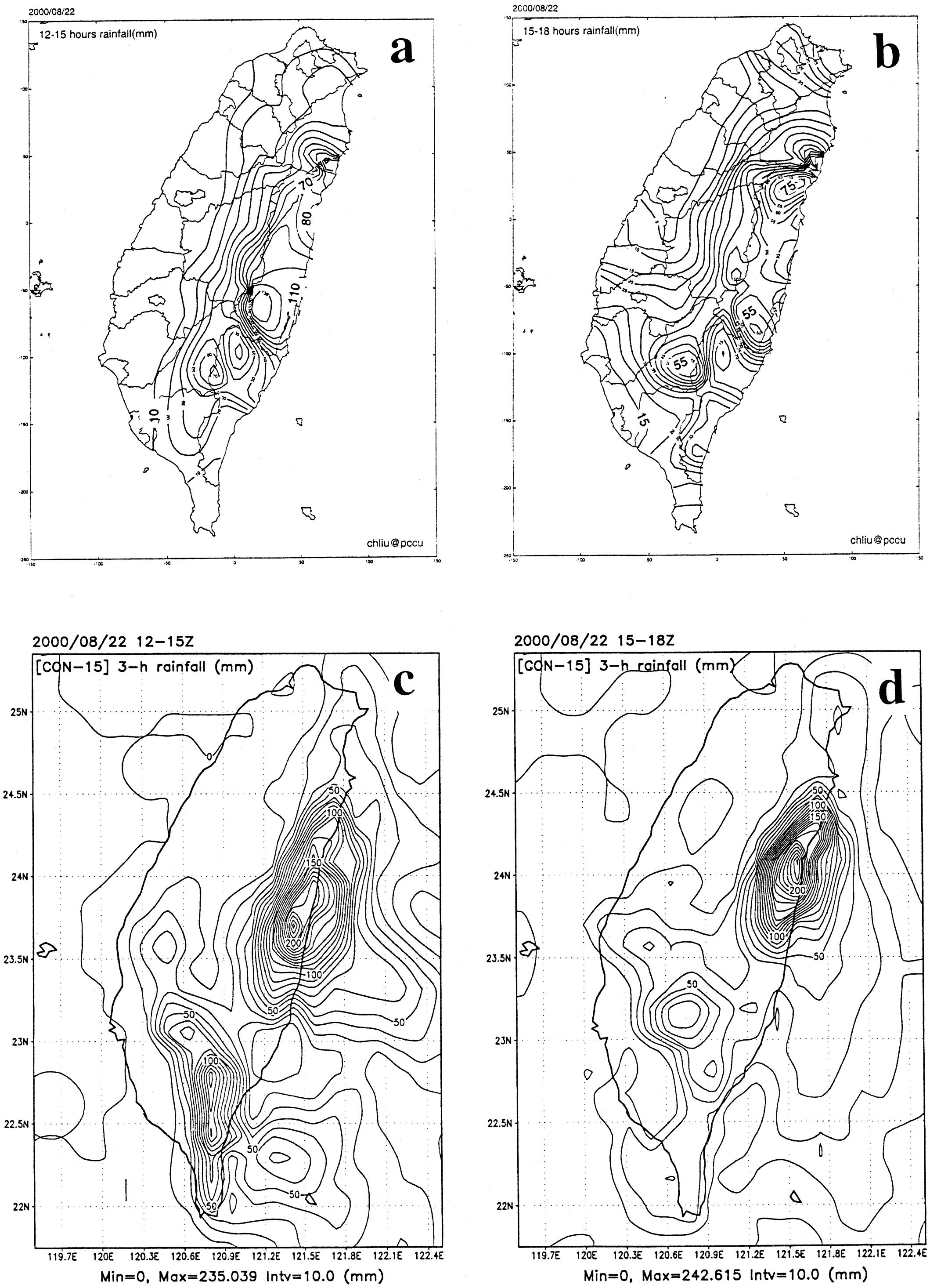

FIG. 9. Observed 3-h accumulated precipitation (in mm) valid for (a) 12–15UTC, and (b) 15–18UTC 22 Aug 2000. The contour intervals are (a) 10 and (b) 5 mm. During 12–15UTC (15–18UTC), the 3-h maximum rainfall is about 110 mm (75 mm) in northeast Taiwan and about 140 mm (60 mm) at central east Taiwan; (c),(d) the corresponding simulated (CON-15) precipitation.

environments of Bilis consisted of a low-level jet impinging on the east coast of Taiwan when Bilis approached the island (see Fig. 6), high moisture, and a conditionally unstable airstream often associated with typhoon circulations. In addition, the CMR has a very steep slope (~3 km/80 km), which helped induce strong upward vertical motion. Thus, most of the above common ingredients were contained in synoptic and mesoscale environments associated with Supertyphoon Bilis. The above common ingredient argument was deduced from the following:

$$P = (\rho/\rho_w)E\,[\mathbf{V}_H \cdot \nabla h + w_{\text{env}}]qL_s/c_s, \qquad (1)$$

where P is the total precipitation (in m), ρ the air density, ρ_w the liquid water density, E the precipitation efficiency, $\mathbf{V}_H$ the low-level horizontal flow velocity, h the mountain geometry, w_{env} the environmentally forced vertical motion, q the water vapor mixing ratio, L_s the horizontal scale of the convective system, and c_s the propagation speed of the convective system.

In order to apply this argument to the prediction of heavy orographic rainfall formation and distribution, Lin et al. (2001) also proposed an index based on the *orographic moisture flux*, which for a two-dimensional flow is simply $U(\partial h/\partial x)q$, and which is similar to that proposed by Alpert (1986). In order to include the vertical moisture flux induced by the environmentally (i.e., synoptically) forced vertical motion and that induced by flow convergence over a flat surface, we propose a *flux model*, which includes both the three-dimensional orographic moisture flux $(\mathbf{V} \cdot \nabla h)q$ and the *general moisture flux wq* of the incoming flow. By assuming $E = 1$, these two moisture fluxes will then give the precipitation rate P. We predict the rainfall distribution from this flux model by using the numerically simulated horizontal wind velocity ($\mathbf{V}$) and moisture (q) fields and subsequently compare it with the observed rainfall distribution.

Figure 10 shows the 850-hPa orographically induced vertical moisture flux $(\mathbf{V} \cdot \nabla h)q$ and the general vertical moisture flux wq, respectively, from the CON-15 simulated results for 8/22/12UTC and 15UTC. Surprisingly, positive areas of both of these two moisture fluxes agree very well with the observed rainfall pattern (Figs. 9a,b) except for a 3-h time lag. Both show elongated positive areas with local maxima along the east coast of Taiwan. The heavy rainfall over the peninsula of southern Taiwan, as predicted by the CON-15, is not present in these two moisture fluxes. In the period of 15–18UTC, positive areas of both of these two fluxes (Figs. 10b,d) propagated northward along the east coast of Taiwan, which is consistent with observations (Fig. 9b). The consistency between the observed rainfall distribution and that predicted by the moisture flux model indicates that the rainfall, which occurred over the mountains, was strongly controlled by the orographic forcing rather than by the original rainbands associated with the typhoon. The time lag (which is not exactly 3 h as indicated here) is the time required for the numerically simulated microphysical processes to activate in the model in order to produce rainfall, similar to that adopted in wave–CISK (conditional instability of the second kind) models (e.g., Davies 1979). Over the ocean, the positive areas of 850-hPa general vertical moisture flux (wq; Figs. 10c,d) correlate well with the locations of the simulated 3-h accumulated precipitation distribution (Figs. 9c,d), since the rainfall over the ocean (and sometimes along the shoreline) was mainly initiated by low-level convergence. The correlation between the general moisture flux and the low-level divergence is reasonably good (Fig. 11).

Figures 12a,b illustrate the predicted 3-h accumulated rainfall in the 5-km simulation (CON-5) for the periods of 8/22/12–15UTC and 15–18UTC, respectively. The CON-5 simulation (Figs. 12a,b) better predicted the observed local maximum rainfall regions (Figs. 9a,b) compared to CON-15 (Figs. 9c,d). Similar to the predicted 24-h accumulated rainfall (Fig. 8c), total rainfall amounts were overpredicted. Note, however, that the rainbands associated with Bilis over the ocean are well predicted by the CON-5 simulation. The orographically induced moisture flux $(\mathbf{V} \cdot \nabla h)q$ (Figs. 13a,b) and the general vertical moisture flux wq (Figs. 13c,d) calculated from the CON-5 simulation showed a significantly more detailed structure, but did not necessarily compare better with the observations than those calculated from the CON-15 simulation results (Fig. 10).

If the duration time of the storm, L_s/c_s, can represent the total precipitation period, then the total precipitation (P) may be roughly estimated by multiplying the moisture flux with the duration time by assuming $\rho = 1$ kg m^{-3}, $\rho_w = 10^3$ kg m^{-3}, $E = 1$, and $w_{\text{env}} = 0$ m s^{-1}, according to Eq. (1). Based on this argument, then, the maximum accumulated precipitation for the period from 8/22/12UTC to 15UTC as predicted by the moisture flux model using results from the CON-15 simulation are roughly 26 mm for the orographically induced vertical moisture flux (Fig. 10a) and 39 mm for the general moisture flux (Fig. 10c), respectively. Compared with their observed values of 140 and 75 mm, respectively, the total rainfall is far underpredicted by the flux model. This discrepancy is due to the neglect of the upward vertical motion triggered by CAPE when the conditionally unstable air is lifted by the mountains. The maximum rainfall predicted by the flux model using results from the CON-5 simulation is greater, 76 mm for the orographic vertical moisture flux (Fig. 13a) and 72 mm for the general vertical moisture flux for the period 8/22/12–15UTC, values which are still underpredicted.

Due to the fact that coarser horizontal-resolution model predictions have a larger lead time compared to finer-horizontal-resolution model predictions, we propose that the orographically induced and general moisture fluxes calculated from Eq. (1) using wind and moisture fields from a coarse mesh simulation can be used to help identify potentially heavy orographic rainfall

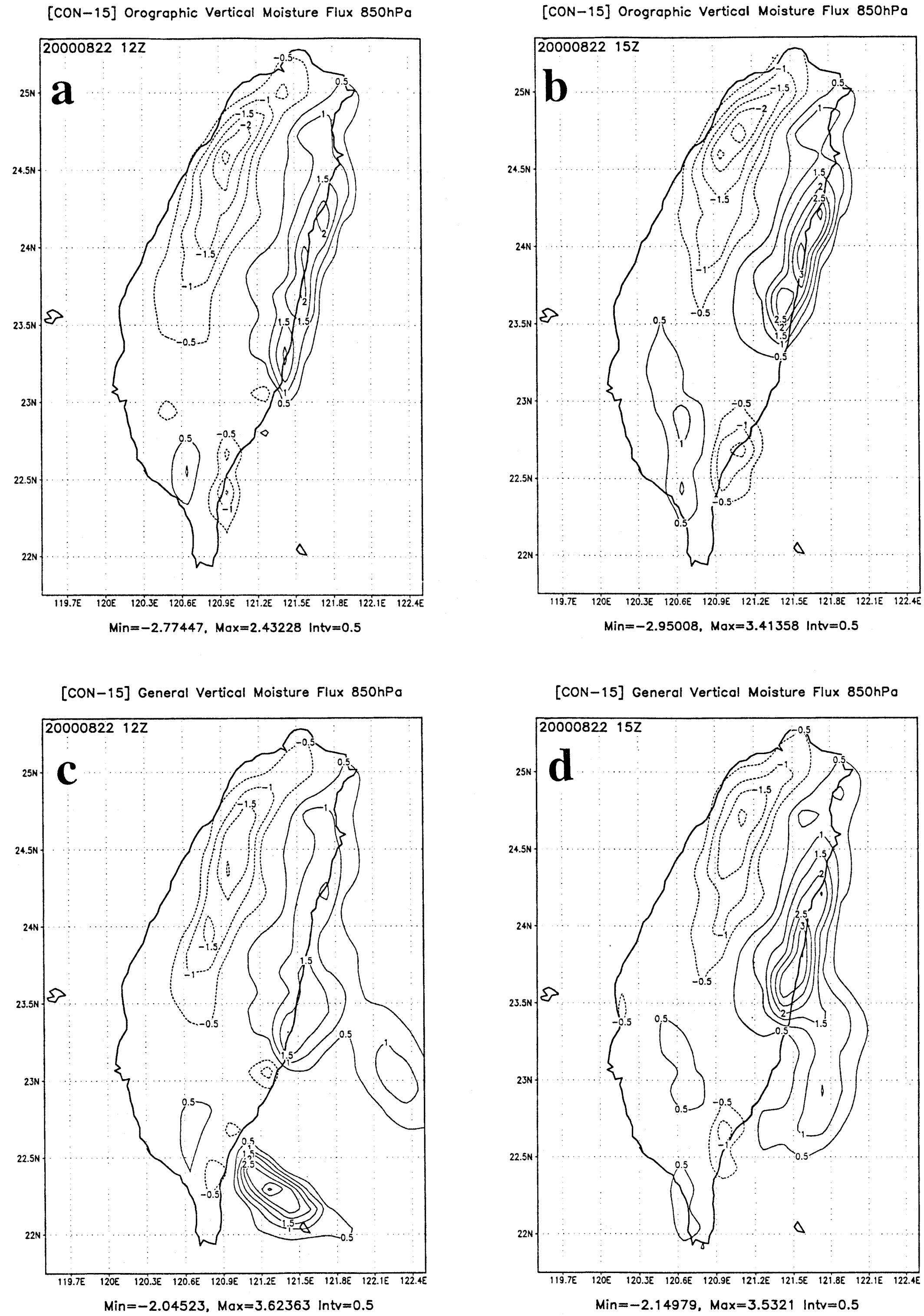

FIG. 10. Orographically induced vertical moisture flux $(\mathbf{V} \cdot \nabla h)q$ [in (m s^{-1})(g kg^{-1})] valid at (a) 8/22/12UTC and (b) 8/22/15UTC. The calculations are based on simulated results of CON-15; (c),(d) the corresponding general vertical moisture flux (wq).

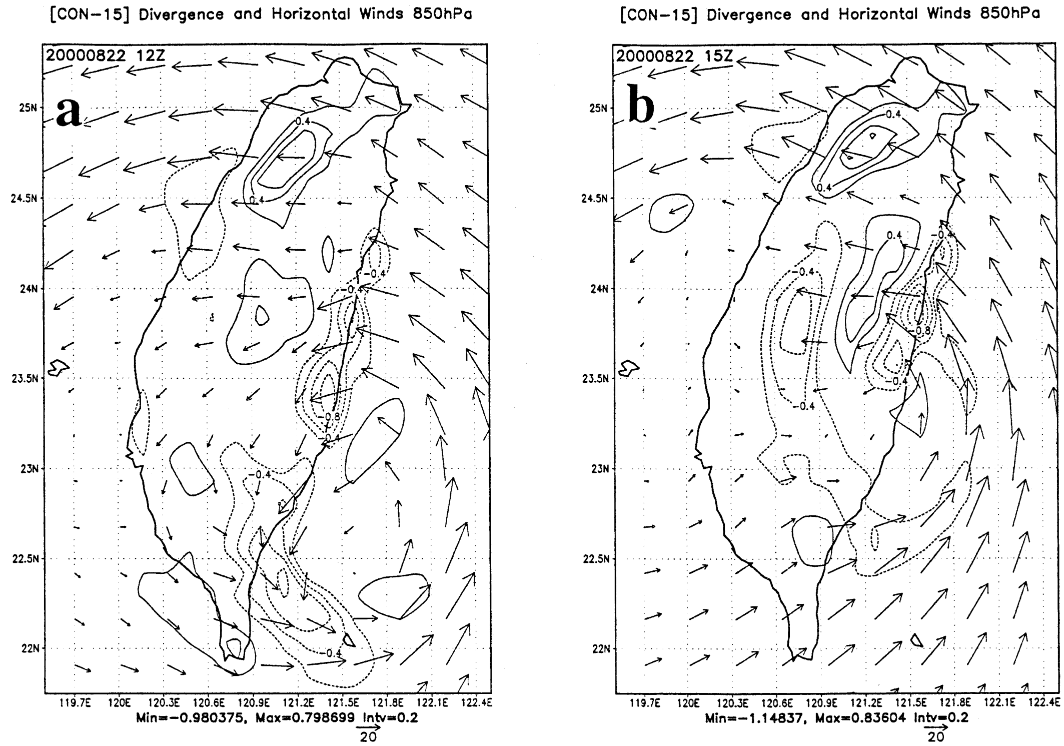

FIG. 11. Simulated (CON-15) 850-hPa divergence (in 10^{-3} s^{-1}) and horizontal vector wind fields at (a) 8/22/12UTC and (b) 8/22/15UTC. Note that dashed lines denote convergence areas.

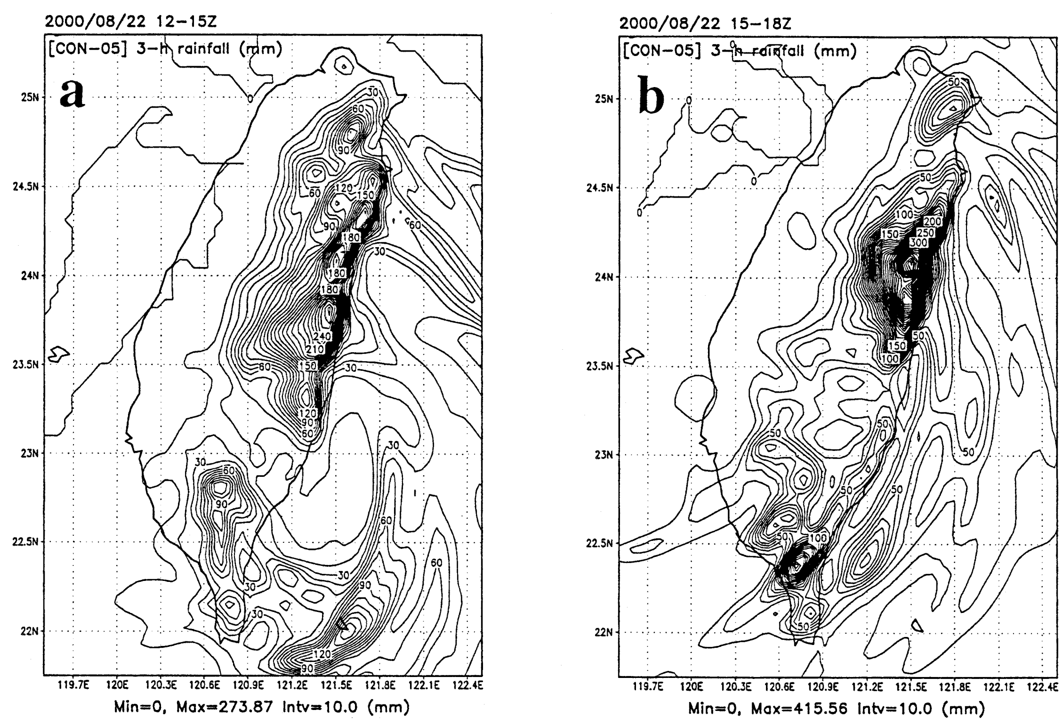

FIG. 12. Simulated (CON-5) 3-h accumulated precipitation (in mm) valid for (a) 12–15UTC and (b) 15–18UTC 22 Aug 2000.

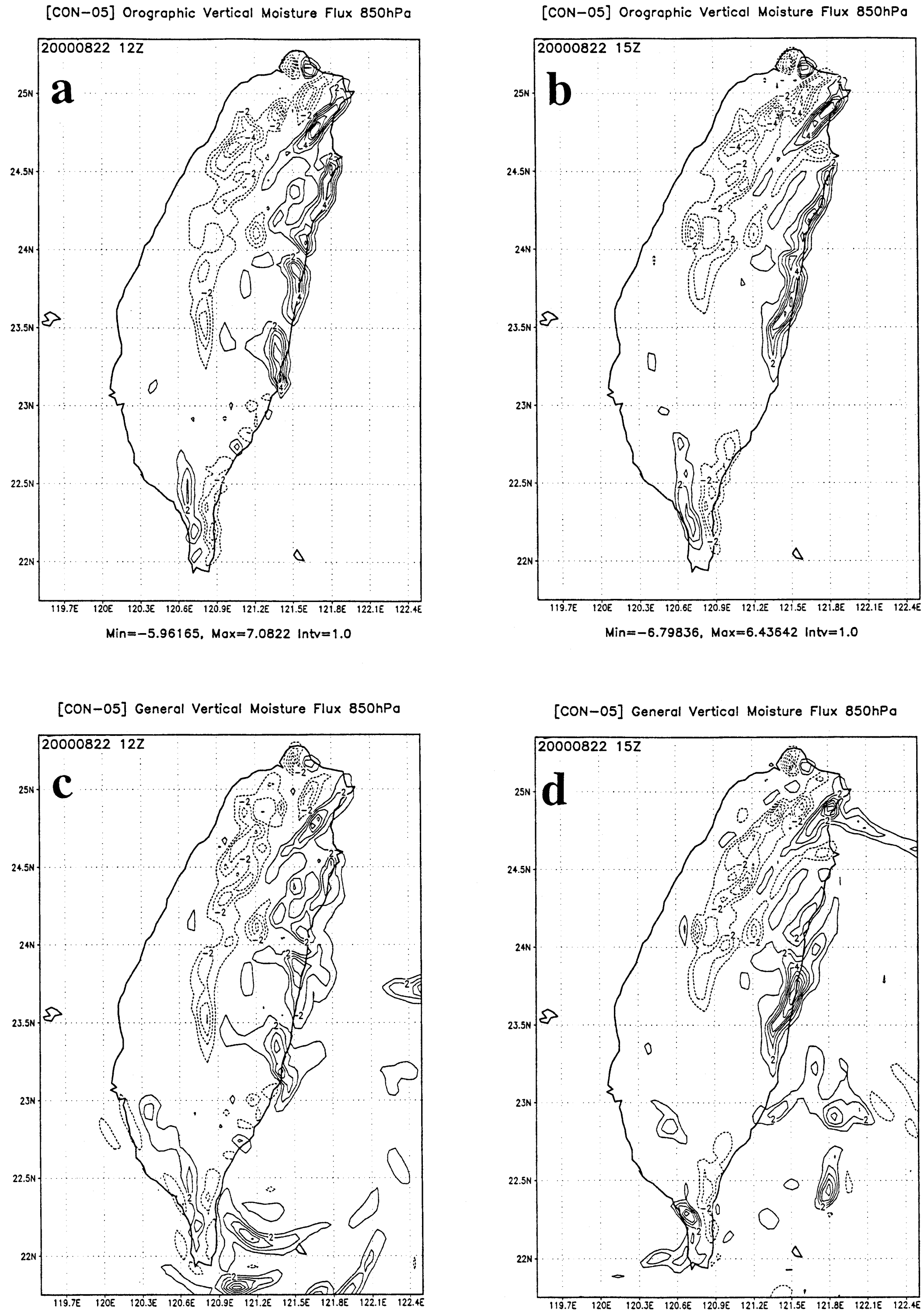

FIG. 13. Orographically induced vertical moisture flux $(\mathbf{V} \cdot \nabla h)q$ [in (m s^{-1})(g kg^{-1})] valid at (a) 8/22/15UTC and (b) 8/22/18UTC. The calculations are based on simulated results of case CON-5; (c),(d) the corresponding general vertical moisture flux (wq).

areas. This method can therefore help in the overall prediction of rainfall areas by operational weather forecasters before actual moist, cloud-scale convective processes occurring in the atmosphere can be better parameterized and more realistically represented in mesoscale numerical models.

4. Orographic influence on track deflection of tropical cyclones

In order to identify control parameters for determining the track continuity and deflection for tropical cyclones passing over a mesoscale mountain, we revisited and analyzed results from previous studies of both idealized and real-case numerical simulations, as well as observational analyses for typhoons passing over Taiwan's CMR. The previous studies that were selected are Wang (1980), Chang (1982), Bender et al. (1987), Yeh and Elsberry (1993a,b), Huang and Lin (1997), Lin et al. (1999), CL02, and this study (denoted hereafter as Bilis for the actual observed storm and CON-15 for the simulated storm). The basic flow and orographic parameters chosen are the basic flow speed perpendicular to the mountain (U), the maximum tangential wind of the TC (V_{max}), the radius of the maximum tangential wind (R), the Brunt–Väisälä frequency (N), the maximum mountain height (h), mountain half-widths in both the east–west (L_x) and north–south (L_y) directions, and the Coriolis parameter (f). Based on the above parameters, we have estimated the following potential control parameters, which are not necessarily exclusive and independent of each other: U/Nh, V_{max}/Nh, h/L_x, R/L_x, Nh/fL_x, L_y/L_x, V_{max}/U, U/fL_x, L_x/U, and V_{max}/Rf.

Table 2 summarizes our estimates of values for the above potential control parameters. The only parameters whose magnitudes are directly related to track continuity are V_{max}/Nh, V_{max}/U, and V_{max}/Rf. That is, when V_{max}/Nh, V_{max}/U, and V_{max}/Rf are simultaneously large, such as $V_{max}/Nh > 1.6$, $V_{max}/U > 7.0$, and $V_{max}/Rf > 4.0$, then the TC track is continuous. Otherwise, the TC track is discontinuous. The other parameters do not seem to have a clear relationship with regard to track continuity. To test this hypothesis, we made estimates of the above three control parameters for the observed storm (Bilis) and the simulated storm (CON-15). The observed storm has $V_{max}/Nh = 2.70$, $V_{max}/U = 14.4$, and $V_{max}/Rf = 6.21$ (Table 2). Thus, it falls into the continuous track regime, which is consistent with the best-track analysis shown in Fig. 4. The simulated storm (CON-15) has $V_{max}/Nh = 1.50$, $V_{max}/U = 5.8$, and $V_{max}/Rf = 3.02$ (Table 2). Thus, the flow falls into the discontinuous track regime, which is also consistent with the track shown in Fig. 4. At 8/22/15UTC, two low-pressure centers associated with the simulated CON-15 storm were present: one located upstream of the mountain range and the other located downstream in northwestern Taiwan. Note that storm CON-15 is assessed as a different storm from Bilis, is much weaker in strength, and serves as a sensitivity simulation in this study.

The nondimensional control parameter V_{max}/Nh for track continuity may be regarded as a vortex Froude number of the airstream associated with the typhoon tangential circulation, analogous to the basic-flow Froude number (U/Nh), which measures the degree of linearity of a uniform, stratified flow over topography (Miles and Huppert 1969). The inverse Froude number Nh/U has also often been referred to as the nondimensional mountain height. In a uniform, stratified flow over a bell-shaped (or witch of Agnesi) mountain, upstream blocking occurs when $U/Nh < 0.57$ ($Nh/U > 1.75$). This blocked fluid propagates upstream when $U/Nh \leq 0.5$ ($Nh/U \geq 2$) (e.g., Baines 1987, 91–93). The systematic numerical simulations made by Lin and Wang (1996) identified four flow regimes for two-dimensional stratified flow over a bell-shaped mountain and also showed that blocking is stronger when the basic-flow Froude number decreases (see their Fig. 5). When a TC vortex approaches a north–south oriented mountain range (such as Taiwan's CMR) from the east, the northern part of the tangential wind impinges more perpendicularly on the mountain. Thus, the vortex Froude number V_{max}/Nh measures the ability of the TC circulation to pass over the mountain. That is, when V_{max}/Nh is larger, there are more air parcels associated with the vortex passing over the mountain. Conversely, blocking is stronger and there is more flow associated with the vortex being forced to go around the mountain. This is analogous to the ''flow-over'' regime and ''flow-around'' regime for a three-dimensional dry flow over an isolated mountain (e.g., Smolarkiewicz and Rotunno 1989; Smith and Gronas 1993). Thus, when V_{max}/Nh is large, it is easier for the TC vortex to pass over the mountain because physically, the kinetic energy associated with the impinging, incipient flow is more than enough to overcome the work required to lift the stratified flow against gravity and overcome the orographic potential energy barrier. Therefore the TC track tends to be continuous. Otherwise, low-level blocking decreases the kinetic energy of the incipient flow and, therefore, the impinging stratified fluid no longer has the ability to overcome the potential energy barrier associated with the topography. This situation will make it more difficult for the TC vortex to pass over the mountain and the track tends to be discontinuous.

The control parameter V_{max}/U measures the relative strength of the typhoon vortex compared to the basic flow. In fact, V_{max}/U may also be viewed as the ratio of the vortex Froude number to the basic-flow Froude number, $(V_{max}/Nh)/(U/Nh)$. Thus, a larger (smaller) V_{max}/U represents a stronger (weaker) vortex and, based on the kinetic and potential energy arguments above, makes it easier (more difficult) for the vortex to pass over the mountain, therefore making the TC track continuous (discontinuous). This hypothesis is also valid for the actual, observed storm Bilis as well as the simulated

TABLE 2. Parameters of flow regimes for tropical storms over a mesoscale mountain range.

Case	U (m s^{-1})	V_{max} (m s^{-1})	N (0.01 s^{-1})	h (km)	R (km)	L_x (km)	L_y (km)	f (s^{-1}) (10^{-5})	Deflection	Cont or not	$\frac{U}{Nh}$	$\frac{\mathbf{V}_{max}}{\mathbf{Nh}}$	$\frac{h}{L_x}$	$\frac{R}{L_x}$	$\frac{Nh}{fL_x}$	$\frac{L_y}{L_x}$	$\frac{\mathbf{V}_{max}}{\mathbf{U}}$	$\frac{U}{fL_x}$	$\frac{L_x}{U}$ (1000s)	$\frac{\mathbf{V}_{max}}{R_f}$
1	5	50	0.86	3.0	200	80	190	5.8	N+	C	0.194	**1.94**	0.038	2.5	5.56	2.38	**10**	1.08	16	**4.31**
2	10	50	0.86	3.0	200	80	190	5.8	~0	D	0.388	**1.94**	0.038	2.5	5.56	2.38	**5.0**	2.16	8	**4.31**
3	5	40	1.025	2.5	120	100	150	5.0	S	C	0.195	**1.56**	0.025	1.2	5.13	1.50	**8.0**	1.00	20	**6.67**
4	5	30	0.72	2.0	210	120	240	5.0	N	C	0.347	**2.08**	0.017	1.75	2.40	2.00	**6.0**	0.83	24	**2.86**
5	5	20	1.025	2.5	120	100	150	5.0	S	D	0.195	**0.78**	0.025	1.2	5.13	1.50	**4.0**	1.00	20	**3.33**
6	10	20	1.025	2.5	120	100	150	5.0	S	D	0.390	**0.78**	0.025	1.2	5.13	1.50	**2.0**	2.00	10	**3.33**
7	5	16	0.72	2.0	210	120	240	5.0	N	D	0.347	**1.11**	0.017	1.75	2.40	2.00	**3.2**	0.83	24	**1.52**
8	10	20	1	2.5	180	80	240	5.8	S	D	0.400	**0.80**	0.031	2.25	5.39	3.00	**2.0**	2.16	8	**1.92**
9	5	19	0.51	2.5	135	160	205	5.8	N	D	0.390	**1.49**	0.015	.8.44	1.37	1.28	**3.8**	0.54	32	**2.43**
10	2.5	19	0.51	2.5	135	160	205	5.8	N	D	0.195	**1.49**	0.015	.844	1.37	1.28	**7.6**	0.27	64	**2.43**
11	5	33	0.51	2.5	135	160	205	5.8	N−	C	0.390	**2.59**	0.015	.844	1.37	1.28	**6.6**	0.54	32	**4.22**
12	5	15.6	0.98	3.0	110	75	180	5.8	~0	D	0.160	**0.52**	0.040	1.47	6.90	2.40	**3.1**	1.15	15	**2.46**
13	6	35	0.78	3.0	200	75	180	5.8	N	D	0.256	**1.50**	0.040	2.67	5.38	2.40	**5.8**	1.37	12.5	**3.02**
14	5	72	0.89	3.0	200	75	180	5.8	N	C	0.187	**2.70**	0.040	2.67	6.14	2.40	**14.4**	1.15	15	**6.21**
15	~5	52.4	0.98	3.0						C		**1.75**					**10.5**			
16	~5	36.8	0.98	3.0						D		**1.23**					**7.4**			

* Case descriptions: 1) BTK5: Bender, Tuleya, and Kurihara (1987) with $U = 5$ m s^{-1}; 2) BTK10, same as BTK5 but with $U = 10$ m s^{-1}; 3) HL2, Haung and Lin (1997) ($V_{max} = 40$ m s^{-1}); 4) Chang-2: Chang (1982) ($V_{max} = 30$ m s^{-1}; 5) HL1, same as HL2 but with $V_{max} = 20$ m s^{-1}; 6) HL1F, same as HL1, but with $U = 10$ m s^{-1}; 7) Chang-3, same as Chang-2 with $V_{max} = 16$ m s^{-1}; 8) LHHH, Lin et al. (1999); 9) YE-WIS, YE's case WIS; 10) YE-WIS, same as 9 but with $U = 2.5$ m s^{-1}; 11) YE-IIS, YE's case; 12) CL, Chiao and Lin; 13) CON-15, simulated case in this study; 14) Bilis, observed case in this study; 15) Wang-I, Wang (1980) with $V_{max} = 52.4$ m s^{-1}; 16) Wang-II, same as Wang-I with $V_{max} = 36.8$ m s^{-1}.

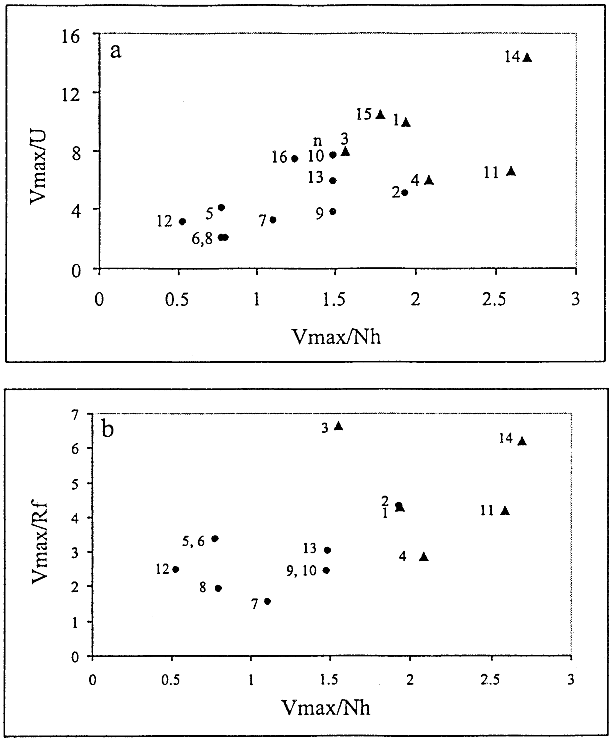

FIG. 14. Continuous (triangles) and discontinuous track (circles) in the parameter spaces of (a) (V_{max}/U, V_{max}/Nh) and (b) (V_{max}/Rf, V_{max}/Nh), based on previous studies of tropical storms over Taiwan's CMR (Table 2).

storm CON-15 (Table 2). The third control parameter V_{max}/Rf is a measure of the ratio of vortex vorticity ($\propto V_{max}/R$) to planetary vorticity (f). Rayleigh's circulation criterion (e.g., see Drazin and Reid 1981) states that a necessary and sufficient condition for inertial (centrifugal) stability of a vortex to axisymmetric disturbances is that the square of the circulation does not decrease anywhere in the field of flow. Thus, the nondimensional parameter V_{max}/Rf may also be considered as a measure of the degree of inertial stability of the TC vortex. When V_{max}/Rf is large (small), the TC vortex is more stable (unstable) and it is easier (more difficult) to pass over the mountain, which tends to result in a more continuous (discontinuous) track. Furthermore, it appears that both V_{max}/U and V_{max}/Rf are directly related to the strength of the vortex and therefore might not be totally independent of each other. In order to examine the dependency of these two nondimensional parameters, that is, V_{max}/U and V_{max}/Rf, we plot them against V_{max}/Nh (Fig. 14). It appears that Figs. 14a,b look very similar, which implies (roughly) that V_{max}/U and V_{max}/Rf are linearly related to each other. Thus, based on an analysis of flow parameters adopted in previous studies, we propose that V_{max}/Nh and V_{max}/Rf may serve as two nondimensional control parameters for determining the track continuity of a tropical cyclone passing over a mesoscale mountain range. However, this hypothesis remains to be justified and more rigorously established by performing systematic, idealized numerical simulations, based on V_{max}/Nh and V_{max}/Rf, and also by estimating these control parameters from observed typhoon cases.

As mentioned in the introduction, Yeh and Elsberry (1993b) found that more intense and rapidly moving typhoons are more likely to cross over mesoscale mountains and thus maintain a continuous track. Their findings regarding the dependence of TC track continuity on vortex intensity appears to be consistent with our analysis of previously mentioned studies. However, the dependence of TC track continuity on the vortex advection speed (which may be represented by U) or the time it takes to pass over the mountain (L_x/U) was not clearly supported by previous studies (Table 2) and observations (e.g., Hsu and Wang 1960; Wang 1980).

Table 2 also indicates that the northward or southward track deflection for a westward-moving TC is related to V_{max}/Nh, but not other parameters. That is, when V_{max}/Nh is large (small), the TC tends to deflect to the north (south). Physically, this means that for a stronger vortex moving in from the east, air parcels associated with the northern portion of the outer circulation of the vortex find it easier to pass over the mountain; therefore, air parcels will follow a more cyclonic track over the mountain, which results in an overall northward deflection of the storm as it passes over the topography. On the other hand, when V_{max}/Nh is small, a greater percentage of the air parcels associated with the outer circulation of the vortex is blocked by the mountain and subsequently deflects the vortex more to the south. Several idealized numerical simulations (e.g., Chang 1982; Bender et al. 1987; Yeh and Elsberry 1993a,b; Lin et al. 1999) have indicated that the TC track is strongly influenced by the steering (basic) flow, which may be represented by the basic-flow Froude number (U/Nh). However, dependence on this control parameter has not been clearly revealed in the parameter analysis of previous studies. Thus, it remains to be examined in future studies, particularly in idealized numerical simulations.

5. Concluding remarks

In this study, we used a nonhydrostatic mesoscale model (COAMPS) to simulate Supertyphoon Bilis (2000) and investigated the dynamics of orographic rain and track deflection affected by Taiwan's Central Mountain Range (CMR). The COAMPS model predicted the storm track as well as the orographic rainfall distribution reasonably well, but overpredicted the total amount of rainfall. The simulated storm turned cyclonically when it passed over the CMR, similar to that found in previous studies. The observed storm track for Bilis is continuous, while the simulated storm track is discontinuous due to its strongly reduced intensity. This reduced storm intensity is mainly caused by the lack of implementing a ''bogus'' vortex initially during model initialization. Thus, the simulated storm was used as a comparison with the actual, observed storm as a model sensitivity test. When the simulated storm approached the east coast of Taiwan, a secondary low developed over the northwestern slopes of the CMR due to compressional adiabatic warming and vorticity stretching, while a secondary vortex formed along the southwestern coast partially due to the northeasterly gap flow between the mountain ranges of Taiwan and China and the easterly gap flow in between the tallest peaks of the CMR.

In general, simulations with both 15- and 5-km horizontal resolution overpredict the total amount of orographic rainfall. We adopt a flux model, as proposed by Lin et al. (2001), to help predict and understand the observed rainfall distribution. Distributions of both the orographic moisture flux and the general vertical moisture flux calculated from the 15-km-resolution model-simulated wind and moisture fields compare reasonably well with the observed rainfall distribution. Results of the flux model using 5-km-resolution model output are not necessarily better than those from the 15-km-resolution model results. Thus, the flux model, along with coarser horizontal resolution model-simulated wind and moisture fields, may be used to help predict the distribution of heavy orographic rainfall associated with landfalling typhoons interacting with mesoscale mountains. The orographic rainfall overprediction problem needs to be addressed in future studies and may be particularly important for the development of better cumulus parameterization schemes than are currently available in mesoscale models, especially for convective precipitation occurring in the vicinity of significant mesoscale topography. The consistency between the observed rainfall distribution and that predicted by the moisture flux model proposed by Lin et al. (2001) indicates that the rainfall that occurred over the mountains was strongly controlled by the orographic forcing, rather than by the original rainbands associated with the typhoon. The total rainfall amounts are underpredicted by the flux model, due to the neglect of upward vertical motion triggered by the release of CAPE associated with the conditionally unstable air.

Analysis of previous studies for tropical cyclones passing over Taiwan's CMR implies that track continuity is strongly linked to three nondimensional control parameters: V_{max}/Nh, V_{max}/U, and V_{max}/Rf. We have found that when values of V_{max}/Nh, V_{max}/U, and V_{max}/Rf are large, such as $V_{max}/Nh > 1.6$, $V_{max}/U > 7.0$, and $V_{max}/Rf > 4.0$, the TC track tends to be continuous. Conversely, TC storm tracks tend to be discontinuous. Estimates of these three control parameters from both the actual, observed Supertyphoon Bilis and its numerically simulated counterpart indicate that the results are consistent with the above finding. Physically, V_{max}/Nh represents the Froude number (or ''linearity'') of the outer circulation of the vortex passing over the mountain, V_{max}/U represents the relative strength of the vortex circulation to the basic flow, and V_{max}/Rf represents the intensity or the inertial stability of the vortex. We hypothesize that when these two parameters are small, kinetic and potential energy conversions associated with orographic blocking force more of the incipient flow to pass around the mountain instead of passing over it. The TC vortex becomes unstable, and the storm track becomes discontinuous. Since V_{max}/U appears to be directly related to V_{max}/Rf, we propose that V_{max}/Nh and V_{max}/Rf may serve as two independent control parameters for determining track continuity. However, this remains to be established more rigorously by performing systematic idealized numerical simulations, based on V_{max}/Nh and V_{max}/Rf, and also by estimating these control parameters from observed typhoon cases. In addition, more precise critical values of these control parameters may be found by performing a more complete suite of numerical experiments encompassing a greater portion of the flow regime diagram than is presented here. These control parameter estimates also imply that the northward or southward track deflection for a westward-moving TC is primarily controlled by V_{max}/Nh, but not the other control parameters. That is, when V_{max}/Nh is large (small), the westward-moving TC tends to deflect to the north (south). This is explained by kinetic and potential energy conversion arguments. The dependence of TC track deflection on the basic-flow Froude number (U/Nh) is not revealed by the control parameter analysis and, therefore, remains to be examined in future studies. Regarding the interaction of the tropical cyclone storm circulation with orography for the subsequent track of the parent cyclone, idealized simulations with more complete physics, especially better numerical representation of moist microphysical and planetary boundary layer processes, are needed.

Acknowledgments. The authors would like to thank Dr. S. Chang at ONR and Dr. J. J. Charney for valuable discussions, and Dr. C.-H. Liu at the PCCU of Taiwan for providing the observed rainfall data. Proofreading of early manuscript drafts by Dr. Charney and some figure plotting by Ms. S.-Y. Chen are also appreciated. The authors would also like to thank Dr. R. P. Weglarz at Western Connecticut State University for his thorough proofreading and valuable comments on the final draft of the manuscript. This study is supported by NSF Grant ATM-0096876. Part of the numerical computations were performed on computers at the North Carolina Supercomputer Center.

REFERENCES

Alpert, P., 1986: Mesoscale indexing of the distribution of orographic precipitation over high mountains. *J. Clim. Appl. Meteor.,* **25,** 532–545.

Baines, P. G., 1987: Upstream blocking and airflow over mountains. *Ann. Rev. Fluid Mech.,* **19,** 75–97.

Bender, M. A., R. E. Tuleya, and Y. Kurihara, 1987: A numerical study of the effect of an island terrain on tropical cyclones. *Mon. Wea. Rev.,* **115,** 130–155.

Chang, S. W.-J., 1982: The orographic effects induced by an island

mountain range on propagating tropical cyclones. *Mon. Wea. Rev.,* **110,** 1255–1270.
Chen, Y.-L., and J. Li, 1995: Characteristics of surface pressure and wind patterns over the island of Taiwan during TAMEX. *Mon. Wea. Rev.,* **123,** 691–716.
Davies, H. C., 1979: Phase-lagged wave-CISK. *Quart. J. Roy. Meteor. Soc.,* **105,** 325–353.
Doswell, C. A., III, H. Brooks, and R. Maddox, 1996: Flash flood forecasting: An ingredient-based methodology. *Wea. Forecasting,* **11,** 560–581.
Drazin, P. G., and W. H. Reid, 1981: *Hydrodynamic Stability*. Cambridge University Press, 527 pp.
Harshvardhan, D. Randall, and T. Corsetti, 1987: A fast radiation parameterization for atmospheric circulation models. *J. Geophys. Res.,* **92,** 1009–1015.
Hodur, R. M., 1997: The Naval Research Laboratory's Coupled Ocean–Atmosphere Mesoscale Prediction System (COAMPS). *Mon. Wea. Rev.,* **125,** 1414–1430.
Hsu, Y. C., and S.-T. Wang, 1960: The problems of typhoon forecasting over Taiwan and its vicinity. *Quart. J. Meteor.,* **2,** 7–12.
Huang, C.-Y., and Y.-L. Lin, 1997: The evolution of a mesoscale vortex impinging on symmetric topography. *Proc. Nat. Sci. Council (Taiwan),* **21A,** 285–309.
Kain, J. S., and J. M. Fritsch, 1993: Convective parameterization for mesoscale models: The Kain–Fritsch scheme. *The Representation of Cumulus Convection in Numerical Models, Meteor. Monogr.,* No. 46, Amer. Meteor. Soc., 165–170.
Kuo, Y.-H., and W. Wang, 1997: Rainfall prediction of Typhoon Herb with a mesoscale model. Preprints, *Workshop on Typhoon Research in the Taiwan Area,* Boulder, CO, National Science Council, 35–45.
Lin, Y.-L., 1993: Orographic effects on airflow and mesoscale weather systems over Taiwan. *Terr. Atmos. Oceanic Sci.,* **4,** 381–420.
——, and T.-A. Wang, 1996: Flow regimes and transient dynamics of two-dimensional stratified flow over an isolated mountain ridge. *J. Atmos. Sci.,* **53,** 139–158.
——, R. D. Farley, and H. D. Orville, 1983: Bulk parameterization of the snow field in a cloud model. *J. Climate Appl. Meteor.,* **22,** 40–63.
——, J. Han, D. W. Hamilton, and C.-Y. Huang, 1999: Orographic influence on a drifting cyclone. *J. Atmos. Sci.,* **56,** 534–562.
——, S. Chiao, T.-A. Wang, M. L. Kaplan, and R. P. Weglarz, 2001: Some common ingredients of heavy orographic rainfall. *Wea. Forecasting,* **16,** 633–660.
Miles, J. W., and H. E. Huppert, 1969: Lee waves in a stratified flow. Part 4: Perturbation approximations. *J. Fluid. Mech.,* **35,** 497–525.
Overland, J. E., and B. A. Walter, 1981: Gap winds in the Strait of Juan de Fuca. *Mon. Wea. Rev.,* **109,** 2221–2233.
Rutledge, S. A., and P. V. Hobbs, 1983: The mesoscale and microscale structure of organization of clouds and precipitation in midlatitude cyclones. Part 8: A model for the ''seeder-feeder'' process in warm-frontal rainbands. *J. Atmos. Sci.,* **40,** 1185–1206.
Scorer, R. S., 1952: Mountain-gap winds: A study of surface wind at Gibraltar. *Quart. J. Roy. Meteor. Soc.,* **78,** 53–61.
Smith, R. B., 1979: The influence of mountains on the atmosphere. *Advances in Geophysics,* Vol. 21, Academic Press, 87–230.
——, and A. Gronas, 1993: Stagnation points and bifurcation in 3-D mountain airflow. *Tellus,* **45A,** 28–43.
Smolarkiewicz, P. K., and R. Rotunno, 1989: Low Froude number flow past three-dimensional obstacles. Part I: Baroclinic generated lee vortices. *J. Atmos. Sci.,* **46,** 1154–1164.
Therry, G., and P. LaCarrere, 1983: Improving the eddy kinetic energy model for planetary boundary layer description. *Bound.-Layer Meteor.,* **25,** 63–88.
Wang, S.-T., 1980: Prediction of the movement and strength of typhoons in Taiwan and its vicinity (in Chinese). National Science Council Research Rep. 108, Taipei, Taiwan, 100 pp.
Wu, C.-C., 2001: Numerical simulation of Typhoon Gladys (1994) and its interaction with Taiwan terrain using the GFDL hurricane model. *Mon. Wea. Rev.,* **129,** 1533–1549.
——, and Y.-H. Kuo, 1999: Typhoons affecting Taiwan: Current understanding and future challenges. *Bull. Amer. Meteor. Soc.,* **80,** 67–80.
Yeh, T.-C., and R. L. Elsberry, 1993a: Interaction of typhoons with the Taiwan topography. Part I: Upstream track deflection. *Mon. Wea. Rev.,* **121,** 3193–3212.
——, and ——, 1993b: Interaction of typhoons with the Taiwan topography. Part II: Continuous and discontinuous tracks across the island. *Mon. Wea. Rev.,* **121,** 3213–3233.
Zehnder, J. A., 1993: The influence of large-scale topography on barotropic vortex motion. *J. Atmos. Sci.,* **50,** 2519–2532.
——, and M. J. Reeder, 1997: A numerical study of barotropic vortex motion near a large-scale mountain range with application to the motion of tropical cyclones approaching the Sierra Madre. *Meteor. Atmos. Phys.,* **64,** 1–19.